

Rotation of Low-Mass Stars in Upper Centaurus Lupus and Lower Centaurus Crux with *TESS*L. M. REBULL,¹ J. R. STAUFFER,² L. A. HILLENBRAND,³ A. M. CODY,⁴ ETHAN KRUSE,⁵ AND BRIAN P. POWELL⁵¹*Infrared Science Archive (IRSA), IPAC, 1200 E. California Blvd., California Institute of Technology, Pasadena, CA 91125, USA;*
*rebull@ipac.caltech.edu*²*Spitzer Science Center (SSC), IPAC, 1200 E. California Blvd., California Institute of Technology, Pasadena, CA 91125, USA*³*Astronomy Department, California Institute of Technology, Pasadena, CA 91125, USA*⁴*SETI Institute, 189 Bernardo Avenue, Suite 200, Mountain View, CA 94043, USA*⁵*NASA Goddard Space Flight Center, Greenbelt, MD 20771, USA*

ABSTRACT

We present stellar rotation rates derived from Transiting Exoplanet Survey Satellite (*TESS*) light curves for stars in Upper Centaurus-Lupus (UCL; ~ 136 pc, ~ 16 Myr) and Lower Centaurus-Crux (LCC; ~ 115 pc, ~ 17 Myr). We find spot-modulated periods (P) for $\sim 90\%$ of members. The range of light curve and periodogram shapes echoes that found for other clusters with *K2*, but fewer multi-period stars may be an indication of different noise characteristics of *TESS*, or a result of the source selection methods here. The distribution of P as a function of color as a proxy for mass fits nicely in between that for both older and younger clusters observed by *K2*, with fast rotators found among both the highest and lowest masses probed here, and a well-organized distribution of M star rotation rates. About 13% of the stars have an infrared (IR) excess, suggesting a circumstellar disk; this is well-matched to expectations, given the age of the stars. There is an obvious pile-up of disked M stars at $P \sim 2$ days, and the pile-up may move to shorter P as the mass decreases. There is also a strong concentration of disk-free M stars at $P \sim 2$ days, hinting that perhaps these stars have recently freed themselves from their disks. Exploring the rotation rates of stars in UCL/LCC has the potential to help us understand the beginning of the end of the influence of disks on rotation, and the timescale on which the star responds to unlocking.

1. INTRODUCTION

The Scorpius-Centaurus OB Association is the closest association to the Sun including massive star formation, and as such, is both important for our studies of young stars, and difficult to study in its entirety because it subtends large angles on the sky, more than 4700 square degrees. In the context of Hipparcos results, de Zeeuw et al. (1999) summarized the literature starting with Kapteyn (1914). Blaauw (1964) broke Sco-Cen into three sub-groups, namely Upper Scorpius or Upper Sco (USco), Upper Centaurus-Lupus (UCL), and Lower Centaurus-Crux (LCC). de Zeeuw et al. (1999) defined boundaries in Galactic coordinates (see Figure 1) for USco ($l \sim 343 - 360^\circ$, $b \sim 10 - 30^\circ$), LCC ($l \sim 285 - 312^\circ$, $b \sim -10 - 21^\circ$), and UCL ($l \sim 312 - 350^\circ$, $b \sim 0 - 25^\circ$, with a ‘bite’ taken out of it to allow for USco¹). It has been difficult to identify members of these groups not only because they cover a large swath of sky, but because this region is in the Galactic plane and close to the Galactic center, so there is a high surface density of non-member (NM) stars.

In recent years, all-sky surveys as well as instruments that can quickly cover large areas of sky have enabled more complete catalogs of members. Gaia (Gaia Collaboration 2016, 2018), in particular, has greatly expanded our knowledge of these clusters. Many groups have recently used Gaia DR2 (Gaia Collaboration 2018) to select USco/UCL/LCC members (e.g., Zari et al. 2018; Goldman et al. 2018; Damiani et al. 2019; Kounkel & Covey 2019; Kerr et al. 2021; and references therein). There are known age and distance differences among the three subgroups – USco is at ~ 143 pc and ~ 11 Myr, UCL is at ~ 136 pc and ~ 16 Myr, and LCC is at ~ 115 pc and ~ 17 Myr (Wright & Mamajek 2018 for distances and Pecaut et al. 2012 for ages, though the ages are still controversial and USco may be as young as 3 Myr – see Rebull et al. 2018 and references therein). We have taken USco here to be ~ 8 Myr based on David et al. (2019).

¹ There aren’t points belonging to UCL ‘hidden’ under the USco box in Figure 1; the vertices of the UCL box are (all in l, b , in degrees): 350, 0; 312, 0; 312, 25; 343, 25; 343, 10; 350, 10; and 350, 0.

There is likely additional substructure within these three broad groupings (see, *e.g.*, Damiani et al. 2019 or Kerr et al. 2021 and references therein), although in the context of this paper, we have limited the groups under consideration to UCL and LCC (and USco from our earlier work).

We have recently been working to understand how the rotational evolution of low-mass stars changes as a function of both age and mass. *K2* (Howell et al. 2014) revolutionized our understanding of this. We have published thousands of *K2* rotation rates from the Pleiades (~ 125 Myr; Rebull et al. 2016a,b, Stauffer et al. 2016b; papers I, II, and III, respectively), Praesepe (~ 790 Myr; Rebull et al. 2017; paper IV), USco/ ρ Oph (~ 8 Myr and ~ 1 Myr, respectively; Rebull et al. 2018; paper V), and Taurus/Taurus Foreground (~ 3 -5 Myr and ~ 30 Myr, respectively; Rebull et al. 2020,2021; Paper VI). Others have also published legions of stellar rotation rates using *Kepler* and *K2* (*e.g.*, Rampalli et al. 2021, Popinchalk et al. 2021, Curtis et al. 2020, and references therein).

Disk lifetimes are mass (and wavelength) dependent but are likely between ~ 2 and ~ 20 Myr (see, *e.g.*, Ribas et al. 2014, 2015), with longer-lived disks around lower-massed stars. USco has a disk fraction of ~ 10 -25% (see, *e.g.*, Luhman & Mamajek 2012) whereas UCL/LCC has a disk fraction of a few percent (see, *e.g.*, Goldman et al. 2018). Exploring the rotation rates of stars in UCL/LCC has the potential to help us understand the beginning of the end of the influence of disks on rotation, and the timescale on which the star responds to unlocking. Since there are several recent papers identifying many thousand members of UCL/LCC, and since NASA’s Transiting Exoplanet Survey Satellite (*TESS*; Ricker et al. 2015) is surveying the whole sky for variability, now is an opportune time to explore the rotation rates of low-mass stars in UCL/LCC to see how they fit in with the rotation rates already known.

We have deliberately performed our analyses of all of our space-based light curves (LCs) and supporting data for stars in all of these clusters, now including UCL/LCC, in as homogeneous a fashion as possible in order to best compare the rotation data across these clusters.

In preparation for discussing the distribution of rotation rates in UCL/LCC, we start by assembling the sample of member stars and defining the member subsamples we use throughout the rest of the paper in Sec. 2. The initial sample is constructed from several papers presenting members, which we then winnow into four sets of targets: gold (the vast majority of the member sample in the end, $\sim 80\%$), silver, and bronze members, and rejected (discarded) targets. These sets are highlighted in tables and figures throughout the paper; the gold sample is the best possible sample, and all the periods (P) measured for these stars are high-confidence. Sec. 3 describes in more detail all the supporting data amassed to enable this analysis, and Sec. 4 describes the *TESS* data, how we deal with confusion and contamination, and how we find and interpret periods in the LCs. Section 5 considers the UCL/LCC sample as a whole and the member subsamples within it. Sec. 6 presents the distribution of periods with color as a proxy for mass for UCL/LCC in context with other clusters, including specifically considering the stars with disks. Finally, we summarize in Sec. 7. There are several Appendices on rejected stars, literature periods, unusual LCs, and timescales.

2. SAMPLE DEFINITION

We start with a set of literature members (Sec. 2.1) and in the end (Sec. 2.3) have four sets of targets that are assembled based on membership confidence and reliability of the linkage between the LC and the star in question: gold (the vast majority of the member sample, $\sim 80\%$), silver, bronze, and rejected (discarded) targets. Gold members have K_s photometry (and either V measured explicitly or an inferred ($V - K_s$)), distances (Bailer-Jones et al. 2018) in the right regime (< 300 pc), and have no indications of source confusion in their *TESS* LC (see discussion below in Sec. 4.2). (It also turns out that the periodic gold members all have highly reliable periods, though that was not imposed upon the sample.) The silver members have all relevant photometry, and only one reason to be concerned about them, which could be a distance that may be too far (see Sec. 3.5) or a suggestion that the LC might be contaminated (see Sec. 4.2). The bronze members have all relevant photometry and two reasons to be concerned. Targets that have three or more reasons to be concerned, or are obviously subject to source confusion, are rejected.

Because we will be referring to these subsamples throughout the paper, we also take the opportunity here to start to put the sample in context (Sec. 2.2) and present all the statistics in one place – see Table 1 for numbers of stars and sample fractions.

2.1. Initial List of Candidate Members

As we have for our *K2* papers (Papers I-VI), we start with an expansive, encompassing list (~ 5300 stars), assembled from the literature as follows.

Because UCL and LCC are relatively nearby, many groups have used Gaia DR2 (Gaia Collaboration 2018) to select members (*e.g.*, Zari et al. 2018; Goldman et al. 2018; Damiani et al. 2019; Kounkel & Covey 2019). Pecaut & Mamajek

(2016) add higher-mass probable UCL/LCC members. For our analysis, we chose to merge the member lists from Zari et al. (2018), Damiani et al. (2019), and Pecaut & Mamajek (2016) to generate our set of UCL and LCC candidates. Note that these papers are based largely on Gaia DR2, not EDR3 (Gaia Collaboration 2021). These lists contain many duplicates with each other, but also many stars that appear in only one list (see Table 1). For Pecaut & Mamajek (2016), we took all stars from their tables 7 or 9 identified as being part of UCL or LCC; note that the the classical boundaries for UCL+LCC from de Zeeuw et al. (1999) were imposed by Pecaut & Mamajek. For Zari et al. (2018), we started with their all-sky pre-main sequence sample and took only those within the de Zeeuw et al. classical UCL+LCC boundaries. Damiani et al. (2019) breaks the population in this region among several subgroups, including clusters that are not UCL/LCC. We took those tagged by them as “LCC” or “D2b” (part of LCC) and within the classical LCC boundaries as members of LCC; for UCL, we took those tagged “UCL” or “D1” (part of UCL) and within the classical UCL boundaries as members of UCL. While Damiani et al. explored a region beyond the classical boundaries, their figure 8 indicates that within these boundaries, we are capturing the overwhelming majority of members. The collection of all of those literature members results in ~ 5300 stars thought to be members of UCL/LCC. We matched this list of stars to numbers from the *TESS* Input Catalog (TIC; Stassun et al. 2018, 2019). Not all of the stars in this initial member catalog have TIC numbers, and not all of the stars with TIC numbers have *TESS* LCs (see Sec. 4). In order for the star to be included in this analysis, however, at minimum, there must be a TIC number, and a LC.

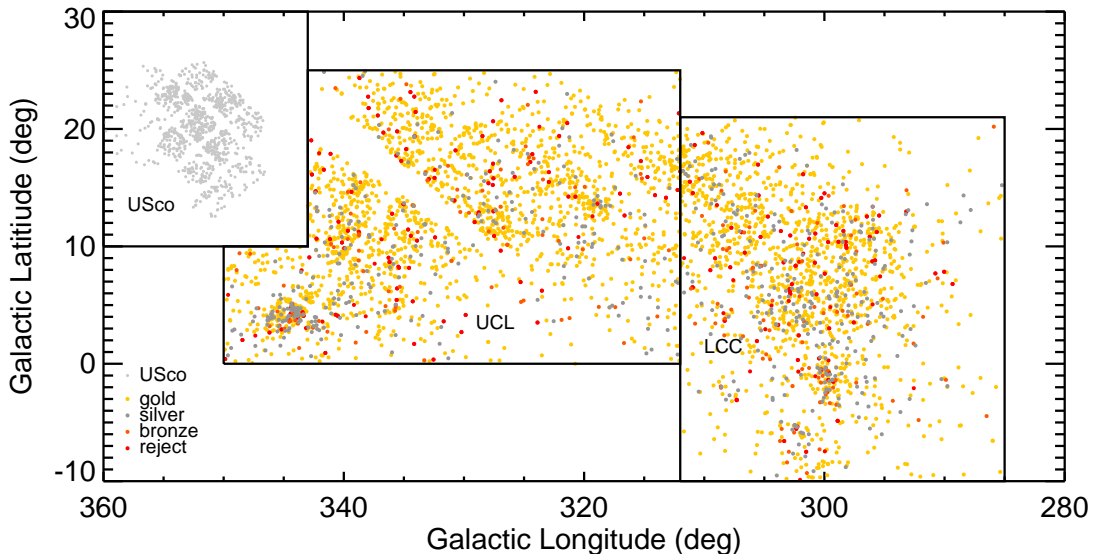


Figure 1. Location of targets in Galactic coordinates. The black lines denote the classical boundaries between USco, UCL, and LCC according to de Zeeuw et al. (1999); see the text. Note that there aren’t points belonging to UCL ‘hidden’ under the USco box. The gold, silver, and bronze members (see Sec. 2.3) are indicated, along with the rejected (discarded) sources (red). The gaps in the spatial distribution are an artifact of *TESS*’ observation strategy. Targets from USco with rotation periods (Paper V) are shown in light grey in the upper left; gaps between the *K2* chips are readily apparent. Note that these regions are in the Galactic plane and near the Galactic center, and as a result, given the large pixel size in *TESS*, source confusion is a concern. Note also that the UCL/LCC member sample is overwhelmingly gold ($\sim 80\%$).

2.2. The Sample In Context

As part of putting this large sample into context, we have included in Table 1 the numbers and sample fractions originating in the three literature membership studies. Note that the sample fractions given there refer to the final sample of 4101 sources presented in Sec. 2.3, as opposed to the ~ 5300 stars described thus far. Figure 1 shows the distribution of our USco stars with rotation periods from *K2* observations (Paper V) in context with the targets from the present paper in UCL/LCC. The classical boundaries between USco, UCL, and LCC (de Zeeuw et al. 1999) are shown. Note that these regions are in the Galactic plane and near the Galactic center, and as a result, source confusion is a concern, especially given the size of *TESS*’ pixels (see Sec. 4). Additionally, IC 2602 is in the lower right of the box

defining LCC, the box defining UCL includes the Lupus clouds, and the USco box includes ρ Oph in the lower center (see, e.g., Figure 8 in Damiani et al. 2019); a few objects from Lupus are incorporated in our member list. Finally, we note that a few of the targets in our list appear in the literature as possible members of TWA, η Cha, ϵ Cha, or USco. There are so many objects that are legitimate members of UCL/LCC that the very few objects that may not be members of UCL/LCC are unlikely to make a significant difference in our analysis.

Figure 2 includes a histogram of K_s (see Sec. 3.1) for this entire set of ~ 5300 stars, for comparison to other subsets presented below (see, e.g., Sec. 4). The literature distribution peaks at $K_s \sim 11$ or 12, which is *very* roughly M4-M5. The faintest literature sources are $K_s \sim 13$.

2.3. Final Culled Sample

The details of winnowing the sample are included later in the paper (Sections 3 and 4), but in summary, the gold sample is the best possible member sample; there is nothing that we can see that stands in the way of working with these stars in this analysis. To the best of our ability to determine, the LC goes with the star we think it does, the star seems to be a legitimate member of UCL or LCC, and the star has all relevant supporting data. Periodic gold stars all have periods in which we have high confidence, although this was not imposed upon the gold sample. Of the members, the vast majority ($\sim 80\%$) are gold members. The silver membership sample has targets that can be worked with in this analysis, but there is one reason to be concerned that maybe the star is not the best possible sample; perhaps there is some question as to whether the star is a member based on distance, or whether the LC is uncontaminated such that it really corresponds to the star we think it does (see Sec. 4.2). The bronze sample has targets with two reasons to be concerned. Rejected targets encompass those that have three or more reasons to be concerned, or incontrovertible evidence that at least at this time, we can't tie a given LC to that star, or we are missing V or K_s photometry (or a LC) such that it isn't possible to include that star in subsequent analysis.

In the remainder of this paper, when we use the term “entire sample,” we mean all of the targets with LCs and ($V - K_s$). When we use the term “all members,” we mean the gold+silver+bronze samples together.

3. SUPPORTING DATA

In this section, we amass supporting data from the literature, including photometry (Sec. 3.1) and spectral types (Sec. 3.2). As for our earlier papers, we wish to use $(V - K_s)_0$ as a proxy for mass, and we continue to do that here, largely using the same approach. The main reason we want to use $(V - K_s)_0$ is to enable comparisons with our other clusters; even though Gaia data are available for essentially all of the entire UCL/LCC sample, Gaia data are not available for all of the stars in the other clusters in Papers I-VI. We describe how we deredden our photometry (where relevant) in Sec. 3.3. We identify IR excesses which we interpret as circumstellar disks (Sec. 3.4). Finally, we describe the distances we used here (Sec. 3.5).

3.1. Literature and Derived Photometry

Based on coordinates from Gaia DR2, for each of our target stars, we obtained corresponding near and mid-IR photometry from 2MASS (Skrutskie et al. 2003, 2006), DENIS (Epchtein et al. 1999, DENIS team 1999), WISE/AllWISE (Wright et al. 2010ab), CatWISE (Eisenhardt et al. 2020, CatWISE team 2020), unWISE (Meisner et al. 2019), Spitzer (Werner et al. 2004) SEIP² (Capak 2013), and AKARI (Murakami et al. 2007, AKARI team 2010ab). We obtained optical broadband photometry from Gaia DR1 (Gaia Collaboration 2016ab) and DR2 (Gaia Collaboration 2018ab), Pan-STARRS DR1 (Chambers et al. 2016), APASS (Henden et al. 2016), NOMAD (Zacharias et al. 2005), the Southern Proper Motion Program (SPM; Girard et al. 2011), and the GSC-II (Lasker et al. 2008). Pecaut & Mamajek (2016) also provide optical magnitudes. We used a typical source matching radius of one arcsecond.

In part as a check on source merging across catalogs, we used all of the photometry to generate a spectral energy distribution (SED) for each source. If the photometric data from one catalog were obviously inconsistent with the rest of the SED, then we removed the data points from that catalog for that source on the assumption that the positional match failed. We also used the IRSA Finder Chart tool (as well as IRSA Viewer) to investigate such source mismatches.

As part of this process, we investigated the WISE and Spitzer (if relevant) images of the target. The WISE objects that were identified as detections but which did not appear obvious in the image and whose detections were not

² <http://irsa.ipac.caltech.edu/data/SPITZER/Enhanced/SEIP/overview.html>

Table 1. Summary of statistics on UCL/LCC sample^a

property	Initial literature	all <i>TESS</i> sources	Gold members	Silver members	Bronze members	all members	NM or rejected sources
count	5264	4101	2978	542	194	3714	387
listed in Zari+	3170 (0.60)	2715 (0.66)	2007 (0.67)	335 (0.62)	124 (0.64)	2466 (0.66)	249 (0.64)
listed in Damiani+	3887 (0.74)	2895 (0.71)	2025 (0.68)	428 (0.79)	152 (0.78)	2605 (0.70)	290 (0.75)
listed in Pecaut&Mamajek16	391 (0.10)	351 (0.09)	289 (0.10)	16 (0.03)	7 (0.04)	312 (0.08)	39 (0.10)
has eleanor LC		3627 (0.88)	2646 (0.89)	437 (0.81)	180 (0.93)	3263 (0.88)	364 (0.94)
has CDIPS LC		3384 (0.83)	2477 (0.83)	437 (0.81)	160 (0.82)	3074 (0.83)	310 (0.80)
has QLP LC		2173 (0.53)	1683 (0.57)	201 (0.37)	69 (0.36)	1953 (0.53)	220 (0.57)
used eleanor LC as best		2533 (0.62)	1789 (0.60)	329 (0.61)	135 (0.70)	2253 (0.61)	280 (0.72)
used CDIPS LC as best		1287 (0.31)	976 (0.33)	180 (0.33)	45 (0.23)	1201 (0.32)	86 (0.22)
used QLP LC as best		281 (0.07)	213 (0.07)	33 (0.06)	14 (0.07)	260 (0.07)	21 (0.05)
V and K_s measured		2934 (0.72)	2249 (0.76)	334 (0.62)	118 (0.61)	2701 (0.73)	233 (0.60)
$(V - K_s)$ via GaiaDR1 $G - K_s$		241 (0.06)	185 (0.06)	29 (0.05)	14 (0.07)	228 (0.06)	13 (0.03)
$(V - K_s)$ via GaiaDR2 $G - K_s$		430 (0.10)	242 (0.08)	105 (0.19)	29 (0.15)	376 (0.10)	54 (0.14)
SED-interpolated V		468 (0.11)	302 (0.10)	74 (0.14)	33 (0.17)	409 (0.11)	59 (0.15)
A_V from JHK_s		1657 (0.40)	1176 (0.39)	255 (0.47)	78 (0.40)	1509 (0.41)	148 (0.38)
A_V from SpTy		97 (0.02)	76 (0.03)	3 (0.01)	1 (0.01)	80 (0.02)	17 (0.04)
median A_V taken		2318 (0.57)	1726 (0.58)	284 (0.52)	115 (0.59)	2125 (0.57)	193 (0.50)
has detected IRAC-1		299 (0.07)	190 (0.06)	62 (0.11)	18 (0.09)	270 (0.07)	29 (0.07)
has detected WISE-1		3904 (0.95)	2940 (0.99)	500 (0.92)	177 (0.91)	3617 (0.97)	287 (0.74)
has detected WISE-3		3742 (0.91)	2846 (0.96)	458 (0.85)	161 (0.83)	3465 (0.93)	277 (0.72)
has detected WISE-4		1146 (0.28)	873 (0.29)	109 (0.20)	44 (0.23)	1026 (0.28)	120 (0.31)
has clear IR excess		354 (0.09)	242 (0.08)	61 (0.11)	20 (0.10)	323 (0.09)	31 (0.08)
has possible IR excess		189 (0.05)	135 (0.05)	26 (0.05)	12 (0.06)	173 (0.05)	16 (0.04)
has any IR excess		543 (0.13)	377 (0.13)	87 (0.16)	32 (0.16)	496 (0.13)	47 (0.12)
obvious source confusion		367 (0.09)	0 (0.00)	0 (0.00)	0 (0.00)	0 (0.00)	367 (0.95)
distance>300 pc		128 (0.03)	0 (0.00)	85 (0.16)	25 (0.13)	110 (0.03)	18 (0.05)
TIC contamination >1.6		434 (0.11)	0 (0.00)	160 (0.30)	178 (0.92)	338 (0.09)	96 (0.25)
mean flux suggests contam		589 (0.14)	0 (0.00)	290 (0.54)	185 (0.95)	475 (0.13)	114 (0.29)
periodic		3640 (0.89)	2693 (0.90)	440 (0.81)	145 (0.75)	3278 (0.88)	362 (0.94)
single P		555 (0.14)	2326 (0.78)	364 (0.67)	126 (0.65)	2816 (0.76)	269 (0.70)
multiple P		555 (0.14)	367 (0.12)	76 (0.14)	19 (0.10)	462 (0.12)	93 (0.24)
periodic+clear IRx		299 (0.07)	204 (0.07)	51 (0.09)	15 (0.08)	270 (0.07)	29 (0.07)
multi-periodic+clear IRx		42 (0.01)	28 (0.01)	7 (0.01)	1 (0.01)	36 (0.01)	6 (0.02)
burster		2 (0.00)	2 (0.00)	0 (0.00)	0 (0.00)	2 (0.00)	0 (0.00)
dipper		56 (0.01)	39 (0.01)	7 (0.01)	0 (0.00)	46 (0.01)	10 (0.03)
dipper+clear IRx		49 (0.01)	39 (0.01)	5 (0.01)	0 (0.00)	44 (0.01)	5 (0.01)
dipper+clear IRx+periodic		48 (0.01)	38 (0.01)	5 (0.01)	0 (0.00)	43 (0.01)	5 (0.01)
double-dip		400 (0.10)	318 (0.11)	24 (0.04)	9 (0.05)	351 (0.09)	49 (0.13)
moving double-dip		28 (0.01)	20 (0.01)	0 (0.00)	2 (0.01)	22 (0.01)	6 (0.02)
shape changer		205 (0.05)	132 (0.04)	29 (0.05)	7 (0.04)	168 (0.05)	37 (0.10)
scallop/clouds? ^b		99 (0.02)	75 (0.03)	8 (0.01)	2 (0.01)	85 (0.02)	14 (0.04)
beater		95 (0.02)	60 (0.02)	4 (0.01)	1 (0.01)	65 (0.02)	30 (0.08)
complex peak		15 (0.00)	10 (0.00)	3 (0.01)	1 (0.01)	14 (0.00)	1 (0.00)
resolved, close peaks		264 (0.06)	170 (0.06)	35 (0.06)	11 (0.06)	216 (0.06)	48 (0.12)
resolved, distant peaks		364 (0.09)	231 (0.08)	54 (0.10)	14 (0.07)	299 (0.08)	65 (0.17)
pulsator		12 (0.00)	6 (0.00)	5 (0.01)	1 (0.01)	12 (0.00)	0 (0.00)

^a Numbers in table are raw number of stars meeting the stated criterion/criteria, followed by the sample fraction within the column in parentheses. For example, 68% of the gold member sample appears as members in Zari et al. (2018); 69% of the entire member sample appears in Damiani et al. (2019).

^b This category includes the scallop shell, persistent flux dip, and transient flux dip categories; see Papers I-VI and Stauffer et al. (2021).

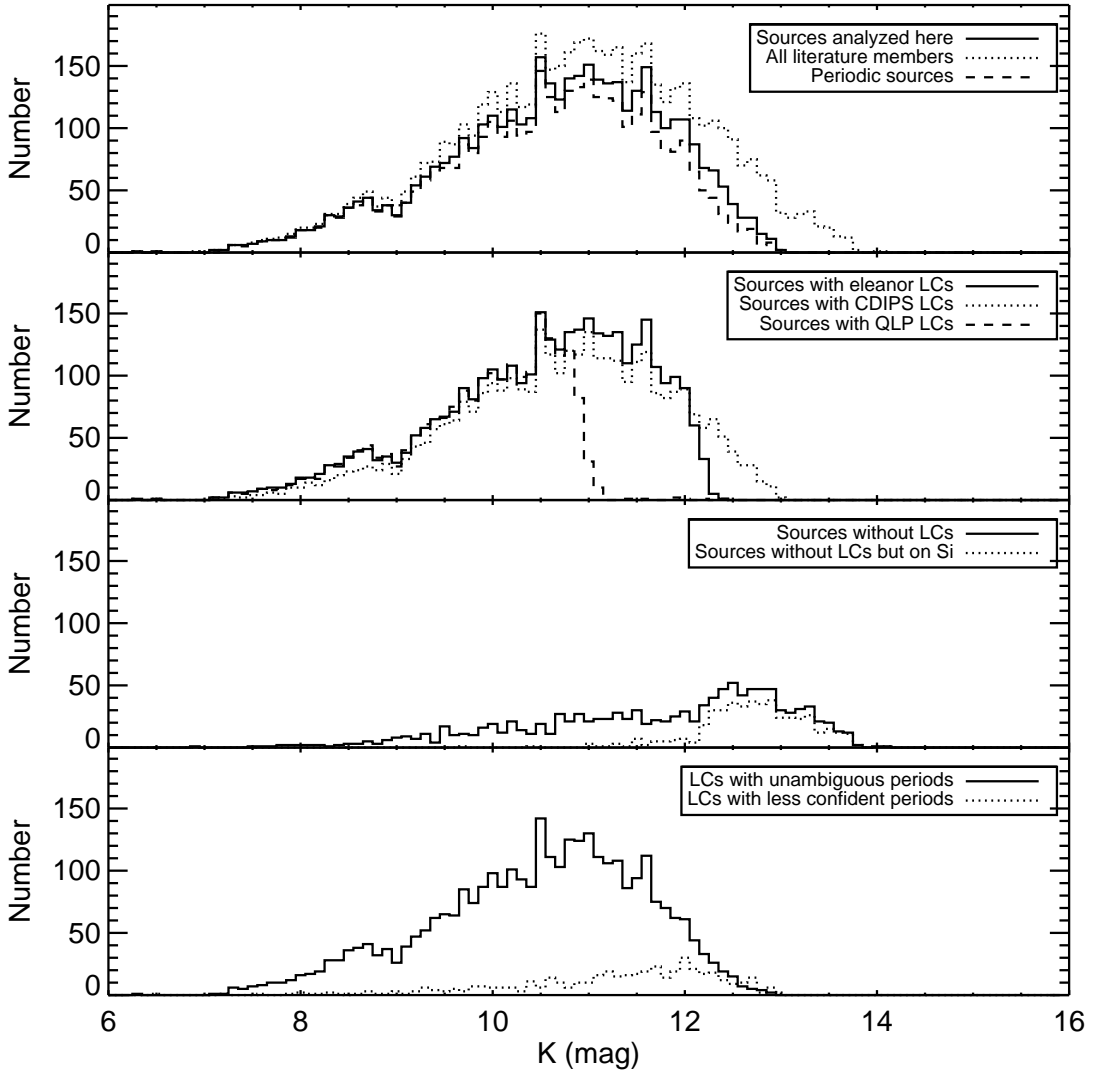


Figure 2. Histograms of brightness (in K_s) of targets in various subsets of data. (Note that y-axis range is the same in all panels.) Top panel: sources analyzed here (solid line) in comparison to all the literature sources identified as likely members of UCL/LCC (dotted line) and the sources identified here as periodic (dashed line). Sources that are missing LCs are biased towards fainter sources. Second panel: sources with *eleanor* LCs (solid line), CDIPS LCs (dotted line), and QLP LCs (dashed line). QLP LCs are biased towards brighter sources, as expected; CDIPS LCs can reach fainter magnitudes than *eleanor* LCs. Third panel: sources without LCs (solid line) and sources without LCs that could, theoretically, exist as the target was on silicon (“on Si”) during *TESS* first year of operations. Targets that are missing LCs are strongly biased towards fainter stars. Fourth panel: sources with LCs that have unambiguous periods (solid line) and LCs where the periods are less confident (dotted line). Targets with less confident periods are on average fainter. Based on these histograms, we conclude most importantly that the selection effect imposed by our requirement that there be a LC does not unduly bias our results; we are missing some of the fainter targets, which is unsurprising.

consistent with the rest of the SED were changed to be upper limits. If Spitzer data existed and the source was visible, but photometry from SEIP was not available, we performed standard aperture photometry on the SEIP mosaics. About 10% of the entire list of sources were missing photometry and were patched in this fashion.

We need $(V - K_s)$ for our target stars to use as a proxy for mass when comparing to other clusters from our Papers I-VI. Essentially all of the stars in our entire sample have measured K_s (see Fig. 2), so we need to find or calculate V . A substantial fraction of the targets have measured V magnitudes in the literature. In cases where V magnitudes were

obtainable from more than one place (APASS, NOMAD, GSC-II, and/or Pecaut & Mamajek 2016), we calculated an average V (see Table 1). Other methods we have used in our other papers ($(V - K_s)$ from Gaia DR1 or V from interpolation of the assembled SED) were necessary in some targets. A few targets missing data from Gaia DR1 but having DR2 necessitated that we derive a new relationship between $(V - K_s)$ and Gaia DR2³. Nearly all of the targets thus have a measured or inferred $(V - K_s)$; see Table 1. However, specifically because we have had to infer $(V - K_s)$ values in many cases, it likely contributes scatter to the distribution.

Stars missing K_s or $(V - K_s)$ cannot be analyzed in the same way as the rest of the entire sample, so those stars are effectively rejected. Most of those missing K_s are blends with nearby stars, so the *TESS* LC is certain to be subject to source confusion anyway (see Sec. 4).

Table 2 includes, for members, the relevant supporting photometric data, including the observed or interpolated $(V - K_s)$, and the IR excess assessments (from Section 3.4), plus the periods we derive (from Section 4). A similar table with all the stars we had to reject appears in Appendix A.

3.2. Spectral Types

We obtained spectral types from Comerón et al. (2009), Skiff (2014), Jang-Condell et al. (2015), Galli et al. (2015), Mellon et al. (2017), Faherty et al. (2018), Goldman et al. (2018) Nicholson et al. (2018), Bowler et al. (2019), Cruzalèbes et al. (2019), Moolekamp et al. (2019; largely photometric types), and Luhman (2022a); finally, if no other types were available, we also consulted SIMBAD⁴ for any additional spectral types. In the end, we have spectral types for less than 20% of the member sample. We have few stars with types earlier than G0, and few later than M6.

3.3. Dereddening

Neither UCL nor LCC have substantial or patchy reddening (see, e.g., Pecaut et al. 2012, Mellon et al. 2017). As in our earlier papers, we placed the stars on a $J - H$ vs. $H - K_s$ diagram, then shifted them back along the reddening law derived by Indebetouw et al. (2008) to the expected JHK_s colors for young stars from Pecaut & Mamajek (2013) or the T Tauri locus from Meyer et al. (1997), and converted to $E(V - K_s)$ via $A_K = 0.114A_V$ (Cardelli et al. 1989). Using this approach, nearly 80% of the member sample has essentially no reddening.

Figure 3 shows a JHK_s color-color diagram for the sample, demonstrating that there is not much reddening for most targets, and for that matter, few optically thick disks in the near-IR (also see Sec. 3.4). (It also shows that all the gold/silver/bronze subsamples are largely similar; we have not preferentially discarded red, or reddened, stars, except for those too faint to have *TESS* LCs.)

We can also start with the spectral type (Sec. 3.2) and compare the observed colors to those expected for that type from Pecaut & Mamajek (2013), from which the reddening can be derived. This approach is less effective here in UCL/LCC because there are so few spectral types known; even among those, there is not much reddening, in general, towards these stars.

We determined or assigned a reddening of 0 to more than half the stars; we took the reddening derived from the JHK_s colors in about 40% of the entire sample (see Table 1). Values of $(V - K_s)$ are included in Table 2 for the members and in Appendix A for the rejected sources. However, as in our earlier papers, to emphasize the net uncertainty, the “vmk0” column in Table 2 has been rounded to the nearest 0.1 mag. The values used in plots here can be recovered by using the $E(V - K_s)$ (“ev-k”) and $(V - K_s)_{\text{observed}}$ (“vk-used”) columns. Table 2 (and its analogous Table 3 for NM) include a 2-digit code indicating the origin of the $(V - K_s)$ value and the method by which the $(V - K_s)$ was dereddened to $(V - K_s)_0$ (see Table 2 or 3 for specific definitions).

3.4. IR excesses

In the process of SED inspection above (Section 3.1), we determined which stars were likely to have unambiguous IR excesses (and therefore likely circumstellar disks in the case of young stars), and noted the wavelength at which the IR excess begins. We noted those with obvious IR excesses (“high confidence”) separately from those where an IR excess might be present (“low confidence” or “possible”; Table 2). A high confidence IR excess might be one where the IR excess is large and detected at more than one wavelength, and/or by more than one instrument; a low-confidence IR excess might be one where the excess is in only one band and where $\chi = (\text{IR color}_{\text{observed}} - \text{IR color}_{\text{expected}}) / (\text{error in}$

³ Where $x = G - K_s$, $V - K_s = -1.383 + 3.554x + (-1.442)x^2 + 0.347x^3 + (-0.026)x^4$. This works well enough for $G - K_s < 5$ and $V - K_s < 7$.

⁴ <http://simbad.u-strasbg.fr/simbad/>

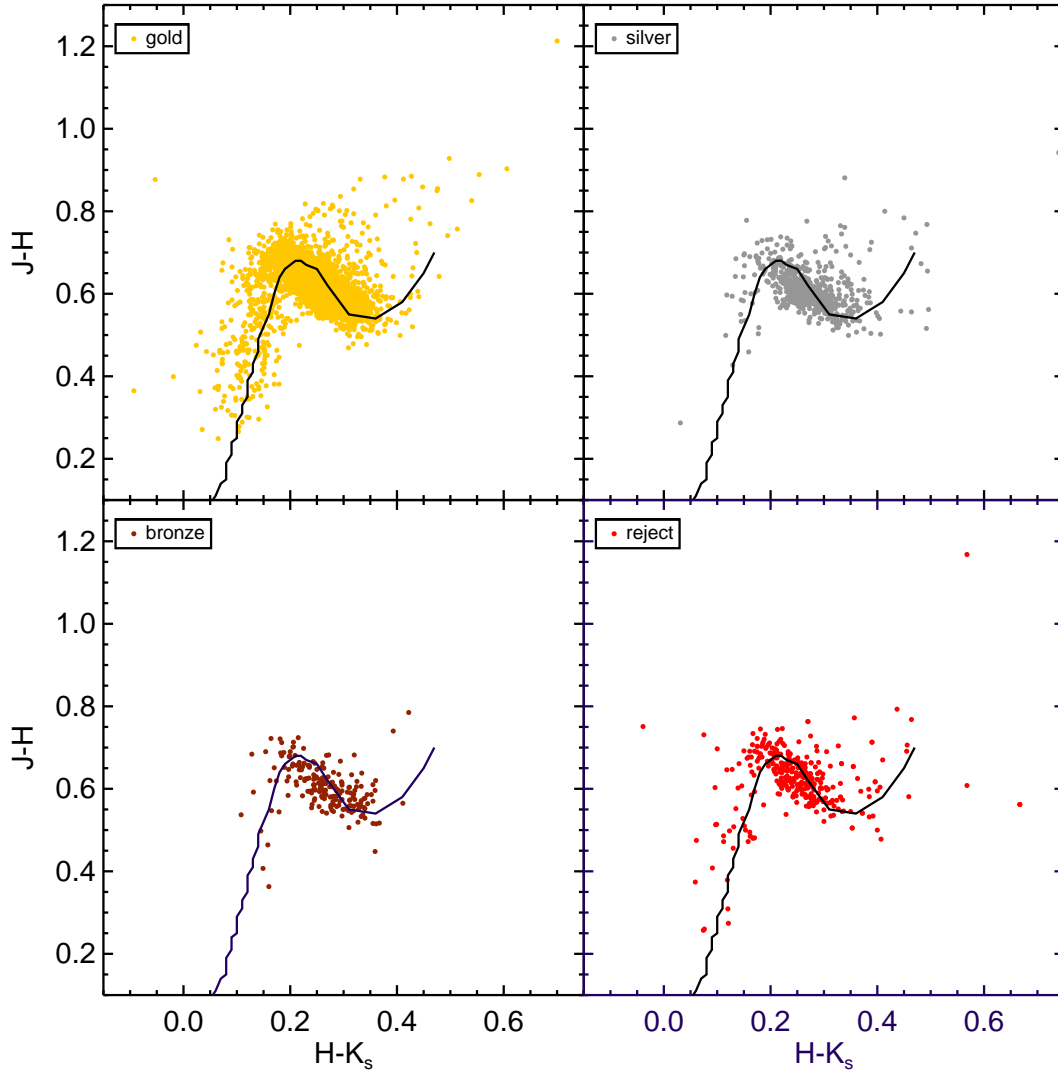


Figure 3. $J - H$ vs. $H - K_s$ (observed) for: upper left: gold members (see Sec. 2.3 for membership); upper right: silver members; lower left: bronze members; lower right: the rejected targets. These plots show both that there is not much reddening on average towards these targets (Sec. 3.3), and moreover that the stars that are being dropped are not particularly or obviously different than the ones that are retained.

IR color) is between 3 and 5. Our source inspection process (Sec. 3.1) ensures that all W3 and W4 detections are secure, so an excess that appears solely at W3 might indeed be real. Just a few percent of the targets have high-confidence IR excesses, and fewer have low-confidence IR excesses (see Table 1). This is consistent with prior determinations of disk fractions in this region (see, e.g., Goldman et al. 2018). Checking against the literature (e.g., Luhman 2022b, Cotten & Song 2016, Mittal et al. 2015, Chen et al. 2014, Carpenter et al. 2009) suggests that our selection mechanism has found the obvious disks, but has indeed missed debris disks with very small IR excesses, which is expected given our approach. To securely and systematically identify subtle excesses would require spectral types and modeling beyond the scope of the present paper.

Spitzer data do not cover the whole region, but WISE data do. WISE detections, even of photospheres, at $12 \mu\text{m}$ are common at this distance, but $22 \mu\text{m}$ limits are also common. Detections from other IR surveys at $\geq 5 \mu\text{m}$ are relatively rare. Figure 4 shows the $[W1]$ vs. $[W1] - [W3]$ for the stars discussed here. Most of the excesses obvious by eye from this plot are selected as high- or low-confidence excesses. The points that are not identified as disks but still

appear in this plot to have significant $[W1]-[W3]$ are stars for which the only indication of an excess is a marginal $[W3]$ detection with a larger-than-typical error bar – that is, they do not have a significant excess.

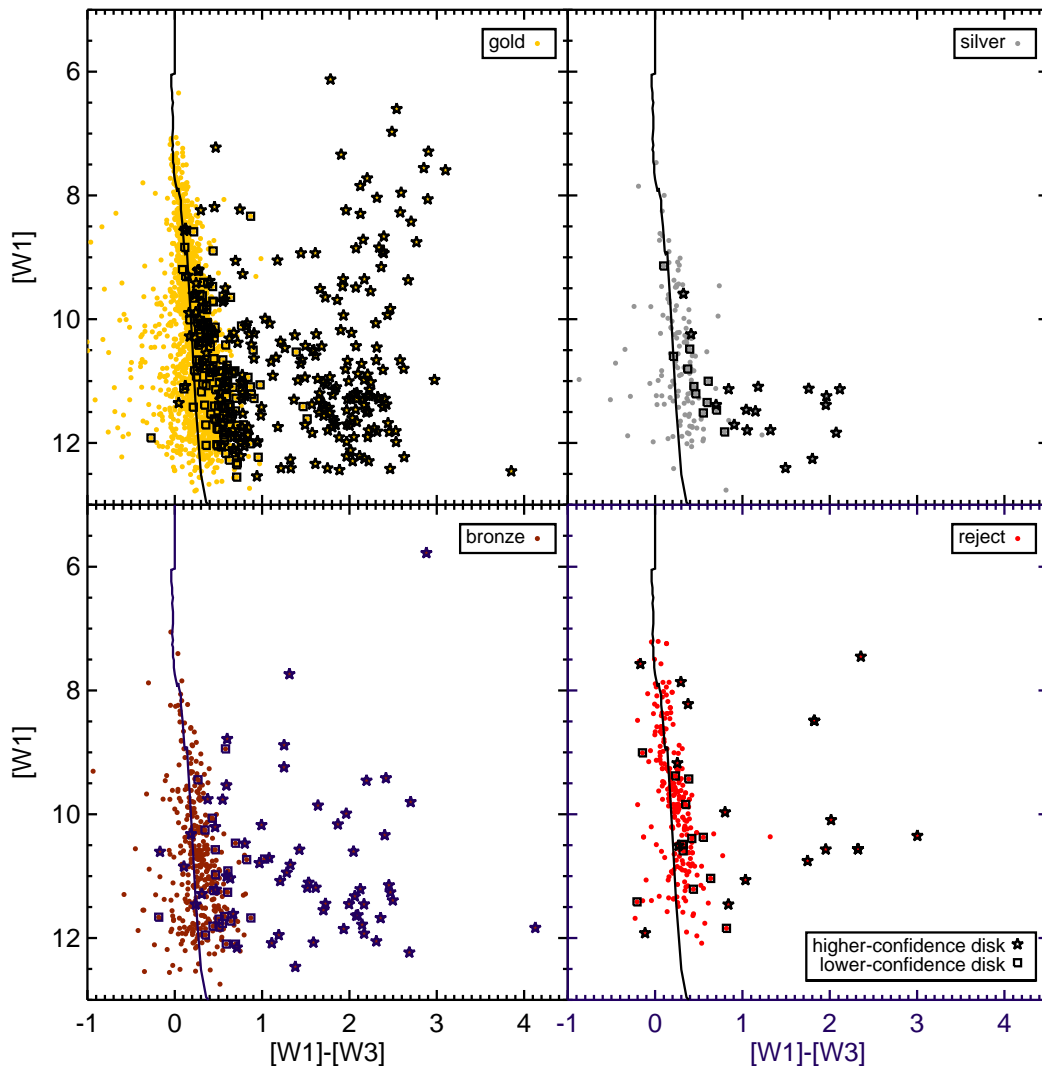


Figure 4. $[W1]$ vs. $[W1]-[W3]$ for the gold, silver, bronze, and rejected targets (see Sec. 2.3). High-confidence disks have an additional star and lower-confidence disks have an additional square. The black line is the expected disk-free colors from Pecaut & Mamajek (2013). The points that are not identified as disks but still appear in this plot to have significant $[W1]-[W3]$ are stars for which the only indication of an excess is a marginal $[W3]$ detection with a larger-than-typical error bar – that is, they do not have a significant excess. Conversely, stars with $[W1]-[W3]$ near 0 but are selected as disks are those that have an IR excess at wavelengths $>12 \mu\text{m}$. Most of the stars with disks are in the gold sample. Disked stars are not preferentially being dropped from the member sample.

Fig. 4 and Table 1 also show that the gold sample has most of the stars with disks (of the stars with unambiguous disks, 68% are in the gold sample); stars with disks are apparently less likely to be at the wrong distance (which makes sense, since young stars in this part of the sky with the right photospheric brightness are more likely than field stars to have IR excesses) or have source confusion issues. We have not preferentially discarded disks; if anything, we seem to have preferentially retained them.

However, our approach for identifying disks is unambiguously biased towards the sources with large excesses. Many of the sources carefully studied with Spitzer (e.g., Chen et al. 2014) were known well before Gaia to be UCL/LCC

members (or simply young), and therefore have much more supporting data in the literature than more recently identified members. The larger net that we have cast has selected stars that for the most part do not have spectral types (Sec. 3.2), and, particularly without that constraint, doing careful assessments of small IR excesses is beyond the scope of the present paper.

3.5. Distances

The distances we used here are those based on Gaia DR2 provided by Bailer-Jones et al. (2018). Since the membership lists we used as input from Zari et al. (2018) and Damiani et al. (2019) both extensively used data from Gaia DR2, we used distances derived from DR2⁵. We expected the members selected in this fashion to all have distances appropriate for UCL/LCC, ~ 100 -200 pc, but for nearly two hundred stars, the distances retrieved from Bailer-Jones et al. are >300 pc. These apparently distant sources are not biased towards, say, those members added from Pecaut & Mamajek (2016), where that analysis was completed pre-Gaia. The distances appear in Table 2 for all members and in Appendix A for the discarded (rejected) sample.

Figure 5 has histograms of the Bailer-Jones et al. (2018) distances for the entire sample as well as the gold, silver, and bronze samples, with an indication of how many stars in those three samples have distances >300 pc. All of the gold sample is <300 pc by definition. A substantial fraction (see Table 1) of the silver sample includes stars that would be in the gold sample, except for their Bailer-Jones et al. (2018) distances. We did not summarily discard these stars because these stars with >300 pc distances were also identified in the literature from Gaia proper motions as belonging to UCL/LCC (see Sec. 2.1). All of these Gaia analyses cannot be simultaneously correct. By way of a specific example, a star known to Simbad as Sz 127 (=TIC 255255634) was selected by Zari et al. (2018) as a member of UCL/LCC. It appears in several papers (e.g., Galli et al. 2013) as a member of Lupus, so historically, it has been regarded as quite close to us (less than a kpc). It has an IR excess, which supports its youth. Simple inversion of the Gaia DR2 parallax yields ~ 160 pc; Bailer-Jones et al. (2018) lists ~ 1640 pc. Because the distances can be wrong, therefore, if any given star has a Bailer-Jones et al. (2018) distance that places it too far away (>300 pc), then that is just one mark against it, as opposed to a reason to reject it entirely.

Our entire sample is biased towards things with Gaia DR2 data, but (in contrast with the other clusters in Papers I-VI), UCL/LCC is sufficiently close and the stars sufficiently not subject to reddening that the bias towards Gaia data is likely to still mean that the sample is representative of the true distribution, at least for sufficiently bright members (earlier than mid-M). Additionally, by discarding (or demoting) those stars that are apparently too far away, simply because they don't represent a large fraction of the sample, we are unlikely to introduce significant bias even if those apparently distant sources really are 100-200 pc away. Kolmogorov-Smirnov (KS) and Anderson-Darling (AD) tests suggest that all the sub-samples in Fig. 5, truncated to <300 pc, are similar to each other; gold and silver are the most different, with silver having fractionally more of the slightly closer sources.

4. TESS DATA

In this section, we obtain *TESS* LC versions from three different pipelines (Sec. 4.1). Source confusion and contamination of LCs is a major concern with *TESS* LCs, and we discuss this in some detail in Sec. 4.2, with some of the mitigation strategies for this developed in the context of looking for periods. The search for periods is presented in Sec. 4.3. In Sec. 4.4, we show that we are obtaining periods at least as reliably as others in the literature, especially for $P < 20$ days. We discuss the interpretation of these periodic signals (Sec. 4.5), and we finish with a summary of the limitations on the range of periods to which we are sensitive (Sec. 4.6).

4.1. TESS LC Versions

A primary driver for inclusion of targets in this analysis is that there be a corresponding *TESS* LC from the first year of the mission. *TESS* covers most of the sky, but not all of it. We used *TESS*-Point (Burke et al. 2020) to assess which of our initial set of stars could possibly have an observed LC in the first year of operations.

We created *eleanor* (Feinstein et al. 2019) 30-minute cadence LCs for most of the candidate members of UCL/LCC from *TESS* LCs from sectors 9-12. This approach provides three versions: PCA, principal component analysis; COR, corrected; and RAW. Some LCs were not successfully extracted, and thus some targets do not have *eleanor* versions.

⁵ Comparing to Bailer-Jones et al. (2021) which uses EDR3, fewer than 40 stars have distances significantly enough different than those from Bailer-Jones et al. (2018) that they would be treated differently here.

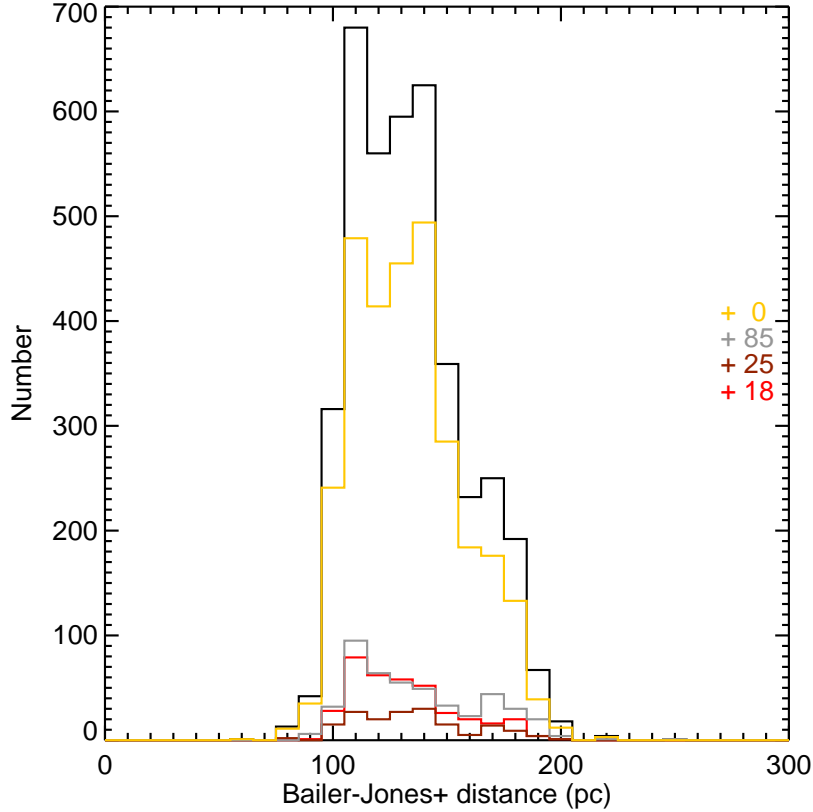


Figure 5. Histogram of distances from Bailer-Jones et al. (2018) from the entire sample (black); the discarded targets (red); bronze, silver, and gold members (see Sec. 2.3). There are additional targets with a Bailer-Jones+ distance >300 , and those are indicated by the correspondingly colored numbers on the far right hand side. Most of the sample (and all of the gold sample) straddles the range of expected distances for UCL/LCC, ~ 100 - 200 pc.

Additional 30-minute cadence LCs from both the Cluster Difference Imaging Photometric Survey (CDIPS; Bouma et al. 2019; <https://doi.org/10.17909/t9-ayd0-k727>) and the MIT Quick-Look Pipeline (QLP; Huang et al. 2020ab; <https://doi.org/10.17909/t9-r086-e880>) were available via MAST, the Mikulski Archive for Space Telescopes. Table 1 includes the numbers and sample fractions of those targets having LCs from each of the three data reductions.

In Figure 1, the obvious stripes of missing sources are primarily an artifact of *TESS*'s observation strategy. There is also an effective cutoff at both the bright and faint ends, where *TESS* saturates or there is an insufficient signal-to-noise ratio. The stars that are missing do not have LCs either because they were not observed in the first year of the mission (“not on silicon”), or largely because they are too faint. The fact that we are missing some fainter stars is unsurprising. Figure 2 includes the K_s brightnesses for the targets analysed here, with separate histograms for sources with *eleanor*, CDIPS, and QLP LCs.

There is no reason to think that the unobserved wedges on the sky would introduce an astrophysical bias. *TESS* has unavoidable bright and faint cutoffs. In practice, the completeness for UCL/LCC falls dramatically for spectral types earlier than late F (no spots to cause periodic modulation) and later than roughly M5 (too faint to have a LC). However, there may be a subtle bias resulting from the fact that we do not have all the *TESS* LC versions for every source. Specifically, the *eleanor* LCs have many more outliers that could mask periods in the LCs, and for many sources are our only choice. In an attempt to counteract the specific issues introduced by photometric outliers, we have spent considerable time on each source to make sure that the best possible LC we have used does not have obvious outliers, and we subsequently identify periods based on cleaned LCs. We are also missing LCs for a few faint sources, even when the target is observable (see Fig. 2), which biases our sample of periods against spectral types later than $\sim M4$ - $M5$.

Table 2. Contents of Table: Periods and Supporting Data for UCL/LCC Members with Viable Light Curves

Number	Column	Contents
1	TIC	Number in the <i>TESS</i> Input Catalog (TIC)
2	coord	Coordinate-based (right ascension and declination, J2000) name for target
3	othername	Alternate name for target
4	gaiaid	Gaia DR2 ID
5	distance	Distance from Bailer-Jones et al. (2018) in parsecs
6	member	membership sample (gold, silver, or bronze)
7	Kmag	K_s magnitude (in Vega mags), if observed
8	vmk-used	$(V - K_s)$ used, in Vega mags (observed or inferred; see text)
9	evmk	$E(V - K_s)$ adopted for this star (in mags; see § 3.3)
10	Kmag0	dereddened $K_{s,0}$ magnitude (in Vega mags), as inferred (see §3.3)
11	vmk0	$(V - K_s)_0$, dereddened $V - K_s$ (in Vega mags), as inferred (see § 3.3; rounded to nearest 0.1 to emphasize the relatively low accuracy)
12	color_uncertcode	two digit uncertainty code denoting origin of $(V - K_s)$ and $(V - K_s)_0$ (see §3.1 and 3.3): First digit (origin of $(V - K_s)$): 1= V measured directly from the literature (including SIMBAD) and K_s from 2MASS; 2= V from the literature (see §3.1) and K_s from 2MASS; 3= $(V - K_s)$ inferred from Gaia DR1 G and K_s from 2MASS (see §3.1); 4= $(V - K_s)$ inferred from Pan-STARRS1 g and K_s from 2MASS (see §3.1); 6= V inferred from well-populated optical SED and K_s from 2MASS (see §3.1); 7= $(V - K_s)$ inferred from Gaia DR2 G and K_s from 2MASS (see §3.1); -9= no measure of $(V - K_s)$. Second digit (origin of $E(V - K_s)$ leading to $(V - K_s)_0$): 1=dereddening from JHK_s diagram (see §3.3); 2=dereddening back to $(V - K_s)_0$ expected for spectral type; 3=dereddening from SED fits; 4=used median $E(V - K_s)=0$ (see §3.3); -9= no measure of $E(V - K_s)$
13	P1	Primary period, in days (taken to be rotation period in cases where there is > 1 period)
14	P2	Secondary period, in days
15	P3	Tertiary period, in days
16	P4	Quaternary period, in days
17	p_uncertcode	uncertainty code for period – is there any reason to worry about this period? Values are ‘n’ (no worry, full confidence; by far the most common value), ‘n’ (no period), and then ‘n?’ and ‘y?’ are progressively less confident periods.
18	IRexcess	Whether an IR excess is present or not (see §3.4)
19	IRexcessStart	Minimum wavelength at which the IR excess is detected or the limit of our knowledge of where there is no excess (see §3.4)
20	SEDslope	best-fit slope to all detections between 2 and 25 microns
21	SEDclass	SED class (I, flat, II, or III) based on the SED slope between 2 and 25 microns
22	dipper	LC matches dipper characteristics (see §4.5)
23	burster	LC matches burster characteristics (see §4.5)
24	single/multi-P	single or multi-period star
25	dd	LC and power spectrum matches double-dip characteristics (see §4.5)
26	ddmoving	LC and power spectrum matches moving double-dip characteristics (see §4.5)
27	shapechanger	LC matches shape changer characteristics (see §4.5)
28	beater	LC has beating visible (see §4.5)
29	complexpeak	power spectrum has a complex, structured peak and/or has a wide peak (see §4.5)
30	resolvedclose	power spectrum has resolved close peaks (see §4.5)
31	resolveddist	power spectrum has resolved distant peaks (see §4.5)
32	pulsator	power spectrum and LC match pulsator characteristics (see §4.5)
33	scallop	LC matches scallop or flux dip characteristics (see §4.5 and App. C)
34	EB	LC has characteristics of eclipsing binary (see §4.5 and App. C)

4.2. Confusion and Contamination

Because the *TESS* pixels are $20'' \times 20''$, source contamination is a concern, especially given that UCL/LCC are in the Galactic plane and located towards the Galactic center. In Papers I-VI, based on *K2* data, assessment of cluster membership was the dominant issue in assembling our final best set of targets and LCs to be analyzed. In the case of UCL/LCC, membership concerns play a more minor role, while source contamination becomes a much more significant concern when assembling the final best sample for analysis.

Because each LC was inspected by hand in order to look for periods (Sec. 4.3), in RA order, there were LCs that we noticed immediately were identical to another nearby (in projection) source’s LC in the set of candidate members. In the past, with the *K2* LCs (Papers I-VI), we have been reasonably successful at teasing apart, through careful data reduction, the periods corresponding to each of any potentially confused targets, though we were unable to do so in

a few cases. However, because the *TESS* pixels are so large, we have had to abandon in most cases here, the hope of attaching individual periods to confused targets with much confidence. Thus, any stars where the LCs were identical to another nearby UCL/LCC star were discarded, without further analysis or discussion, except for the rare occurrence where the stars were of much different brightnesses. In those cases, the period was attached to the brighter star, and the fainter star was discarded.

The total numbers of stars so affected are given in Table 1, and they make up the majority of the discarded (rejected) sources.

Stassun et al. (2018, 2019) assembled, as part of the TIC, a metric that attempts to quantify the degree to which the *TESS* LC is likely to be contaminated by nearby stars and reported it as a contamination ratio. This was assembled pre-launch, and makes a number of assumptions, so we did not rely solely on this value, but it was included in our assessment of whether to believe the *TESS* LC. Figure 6 shows the distribution of this contamination ratio for our targets as a function of brightness. Based on this and other similar plots, we decided that a TIC contamination ratio of 1.6 was an appropriate cutoff; targets with a contamination ratio >1.6 have a mark against them. As for our treatment of distances above, the contamination flag could be unreliable, and so we downgrade (add a mark against) but do not a priori discard sources having a high TIC contamination ratio.

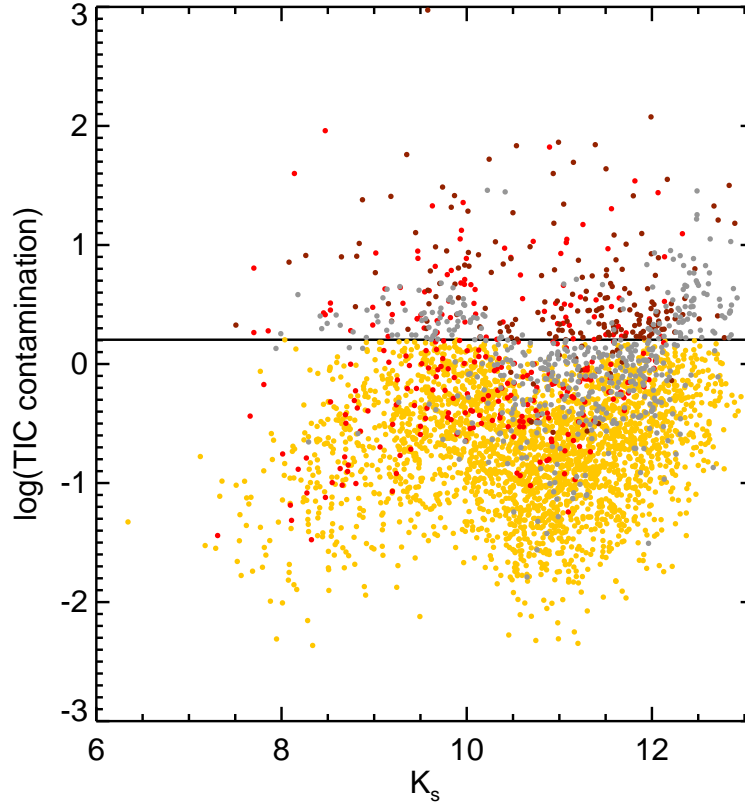


Figure 6. The log of the contamination ratio from the TIC (Stassun et al. 2018, 2019) plotted against K_s . The discarded targets are red; bronze, silver, and gold members are colored correspondingly. The horizontal line is at a contamination ratio of 1.6, a number we arrived at by inspection (of this and other similar plots) as a reasonable cut-off between the LC is “likely contaminated” and “likely not or at least less likely to be contaminated.” Gold members (by definition) have a contamination ratio <1.6 .

Stauffer et al. (2021), in looking for UCL/LCC members that were uncontaminated scallop shell stars, used a quick assessment of contamination. They compared the mean PCA flux in the LC to the Gaia DR2 G mag. Figure 7 does this for the ensemble in order to identify those LCs whose mean flux seems inconsistent with the target’s measured G mag, suggesting that the LC is contaminated by flux from nearby stars. The black line in the left panel is given by

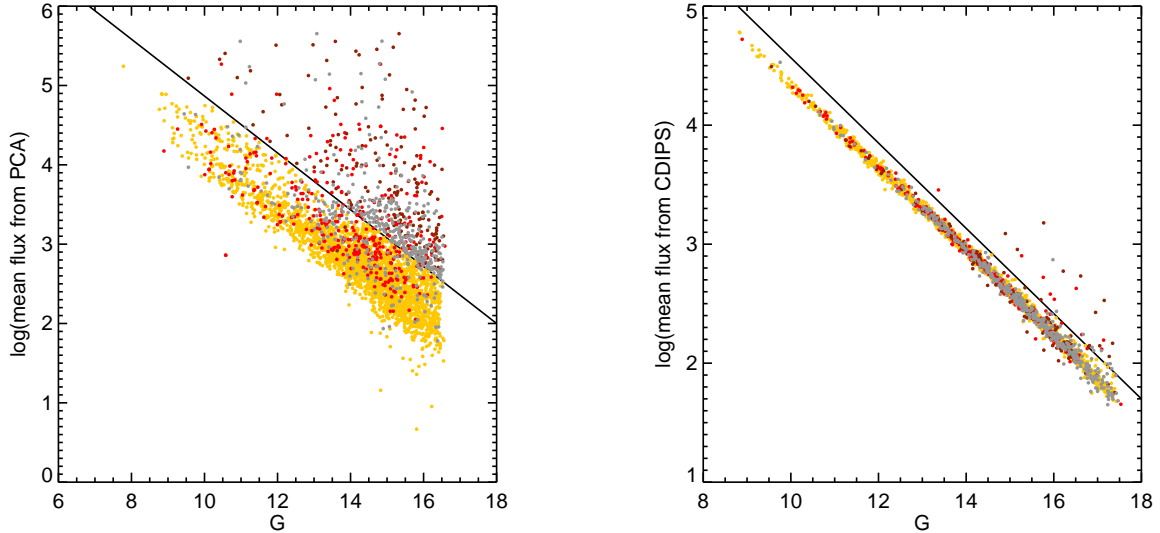


Figure 7. The log of the mean flux from the PCA *eleanor* LCs plotted against Gaia G (left) and the log of the mean flux from the CDIPS LCs plotted against Gaia G (right). The discarded targets are red; bronze, silver, and gold members are colored correspondingly. The black line on the left is given by $\log(\text{mean PCA flux}) = -0.358 \times G + 8.45$ on the left. The black line divides the stars whose G is much different than the mean PCA LC flux from those whose G seems appropriate given their mean PCA flux; stars above this line are likely to be contaminated by neighbors. Gold members (by definition) have a mean PCA flux consistent with their G . Not every one of our targets has an *eleanor* LC, so the right plot repeats the analysis using CDIPS; the black line is the same on the right, just shifted down by 0.3 dex. The scatter is worse for the *eleanor* LCs (left plot) than for the CDIPS LCs (right plot) because there are far more outliers in the *eleanor* LCs.

$\log(\text{mean PCA flux}) = -0.358 \times G + 8.45$. Targets above the black line in Fig. 7 are ones that are tagged as having LCs that are likely contaminated, and those targets accumulate another mark against them. This calculation can also be subject to error, so this criterion is also not enough, on its own, to discard the source. However, a lot of sources that have a high TIC contamination ratio also have an anomalously high PCA flux mean. Most of the sources in the bronze member bin have both a high TIC contamination ratio and a high *TESS* flux compared to the G magnitude (see Table 1).

Because not all of our targets have *eleanor* LCs, we do not have a mean PCA flux for all targets. Figure 7 also includes a similar analysis for the CDIPS LCs. This distribution is far better behaved than it is for the PCA LCs; the black line in this plot has the same slope as that in the PCA plot. There are several reasons why the scatter is worse in the PCA version of this plot than in the CDIPS version. Because the LCs that emerge from the CDIPS analysis have far fewer outliers than the *eleanor* LCs, the mean CDIPS flux is a more accurate representation of the flux from the star. The CDIPS analysis was only performed on a subset of stars that are (a) cluster members, (b) show signs of youth, and (c) have $G < 16$ (Bouma et al. 2019). The *eleanor* LCs were calculated from lists of RA/Dec and likely therefore were extracted even for stars that could be too faint/contaminated to even expect a reasonable LC. Stars that are above the black line in the right panel of Figure 7 are tagged as possibly contaminated, even if they were below the line in the left panel. We note for completeness that the QLP LCs arrive normalized, so the approach adopted for the other LC sets will not work. Therefore, stars that only have a QLP LC cannot be identified as possibly contaminated using this approach.

In summary, the issues arising from *TESS* large pixels are significant. We lose several sources because we cannot identify with certainty which star is the origin of the variation seen in the extracted LC, and/or because effectively the same LC is returned for more than one target in our list. However, there is no reason to think that a significant astrophysical bias would be introduced based on projected distance to a neighbor star bright enough to affect the LC. Later, more sophisticated LC extraction approaches might recover the LCs for some targets. We demoted stars to silver (one mark against), bronze (two marks against), or rejected (three or more marks against) based on how likely we thought it was that the star was too far away (Sec. 3.5) or the LC was contaminated. Despite our best efforts to omit stars where source confusion is significant, it's likely that a few sources subject to source confusion still remain

in our data, even the gold subsample. We anticipate, however, that they are a small minority of the sources used here, particularly in the gold subsample.

4.3. Finding Periods in TESS Data

As in our earlier papers, we selected the ‘best available’ light curve version, this time from the products provided by *eleanor*, CDIPS, and QLP, when available. To identify significant periods, we used the Lomb-Scargle (Scargle 1982) approach as implemented by the NASA Exoplanet Archive Periodogram Service⁶ (Akeson et al. 2013). We also used the Infrared Science Archive (IRSA) Time Series Tool⁷, which employs the same underlying code as the Exoplanet Archive service, but allows for interactive period selection. The period range searched was 0.05 days (1.2 hours) through 20 days. Stars with only one *TESS* sector have about a 30 day campaign (~ 24.1 - 26.9 days for these sectors), suggesting that the maximum plausible period should be about 15 days. About 12% of the targets have more than one *TESS* sector, so $P > 15$ days could be retrievable in those cases. In practice, no periods > 17.1 days were retained as plausible or reasonable.

Each LC was separately inspected by hand. Although an automatic 5σ clipping was imposed, many LCs had significant numbers of extreme outliers. More aggressive automatic clipping both failed to remove all the outliers as well as inappropriately rejected points in LCs that did not have so many outliers. Such problematic outliers were manually removed and the Lomb-Scargle analysis was redone as necessary. The period analysis was also performed with a maximum P of 2 days in an attempt to limit the influence of additional occasional ~ 6 - 7 day timescales in the data that we assume are either instrumental or introduced in data reduction. Stars that appeared to have a period near that regime were subject to particular scrutiny to ensure that they were plausible periods.

We retained up to four viable periods for each target. For the *K2* clusters analyzed in Papers I-VI, about 20% of the stars are multi-periodic, but only $\sim 12\%$ of the members here are multi-periodic. There is no astrophysical reason to assume that the stars in UCL/LCC would be intrinsically less likely to be multi-periodic than the stars in Papers I-VI (which include both older and younger stars). We thus assume that the *TESS* light curves are more difficult to analyze using our approach, perhaps due to increased noise and/or shorter individual campaigns. However, this could be a selection effect. In the *K2* analyses, M stars with multiple periods often turned out to be binaries. The Gaia analyses feeding into our membership lists may have, through the selections made in those papers, biased the samples against binaries (and higher order multiples), so it may be the case that our initial member list is fundamentally less likely to include binaries. Therefore, if most multiple periods are due to stellar multiplicity, our source list is therefore less likely to exhibit multiple periods.

The periods we derive appear in Table 2 for all members and in Appendix A for the discarded (rejected) targets. Note that we have included periods for all the periodic LCs, but for the discarded targets, the periods may very well not correspond to the stars as listed.

For about 10% of the entire sample, there were periods that could be ambiguous; for example, there seemed to be a strong peak in the power spectrum, but the phased light curve was not as convincing as the remaining $\sim 90\%$ of the sample. These are indicated in the corresponding data tables (Tables 2 and 3). They are all fainter targets; see the last panel in Fig. 2 for a histogram comparing the brightness of the high-confidence periods to that of the lower-confidence periods. None of these less-confident periods are found in the gold sample – we note that no star was removed from the gold sample on the basis of having a questionable period.

4.4. Comparison to Literature Periods

As a check on our ability to match stars with the correct LCs as well as retrieve accurate rotation periods, we compare our periods with those in the literature. Four studies monitoring targets in the optical have significant overlap with our targets, and several individual targets appear in a scattering of other papers. Figure 8 presents a comparison of the measured rotation periods, where all stars in common are included, regardless of whether the source is ultimately dropped in our analysis. (Appendix B includes a list of the measured periods for individual comparison, plus notes.)

Kiraga (2012) reported periods from the All Sky Automatic Survey (ASAS). Because the positions as originally reported are not very precise, we took the counterparts as identified in Kiraga (2012), rather than matching anew by position. We have 162 stars in common. Mellon et al. (2017) has 70 stars in common with us; there are a few (see Appendix B) for which they discarded the P they obtained, but we independently recovered it, suggesting that the

⁶ <https://exoplanetarchive.ipac.caltech.edu/cgi-bin/Pgram/nph-pgram>

⁷ <http://irsa.ipac.caltech.edu/irsaviewer/timeseries>

period is real. Gaia DR2 (Gaia Collaboration et al. 2018) included rotation periods, and we have 43 stars in common. The ASAS-SN catalog of variable stars (Jayasinghe et al. 2018) reports periods for 456 stars in common with us. Other rotation period data in the literature can also provide a comparison (Zuñiga-Fernández et al. 2021, Ripepi et al. 2019, Nicholson et al. 2018, Drake et al. 2017, Samus’ et al. 2017, Distefano et al. 2016, Siwak et al. 2016, Desidera et al. 2015, Kóspál et al. 2014, Fruth et al. 2013, Alfonso-Garzón et al. 2012, Donati et al. 2012, Messina et al. 2010, 2011, Broeg et al. 2007, Christiansen et al. 2008, Strassmeier et al. 2005, Batalha et al. 1998, Wichmann et al. 1998). There are a total of 56 such literature stars in common with us. The union of all unique stars in our ensemble that have any period in the literature is nearly 600, about 15% of the ensemble.

The results on the whole are a mix of excellent agreement (the majority), likely harmonics reported in the literature, and for a few, significant disagreement with the periods derived from the high-quality (but often subject to source confusion) *TESS* data. We recover most periods to better than 20%; see percentages in Fig. 8. Limiting the comparison to $P < 20$ days (where we have the highest likelihood of recovering periods with *TESS* data), we recover a higher fraction of periods. In a few cases, the *TESS* light curve has significant variations in the LC such that even a period comparison $>20\%$ could reasonably be considered a match. In some other cases, the literature reports a period similar to one that we had discarded as likely instrumental or less secure (see Appendix B); we did not go back and resurrect our retrieved period, since we do not have the ability to do so for all stars.

For each mismatched period <20 days, we investigated the prior period(s) in comparison to the *TESS* light curve, and we believe that the period(s) we report is/are the correct periods for these stars – or at least the LCs we have associated with them – during the *TESS* campaign(s). Given the relatively coarse sampling rate of ASAS-SN compared to *TESS*, it is perhaps not surprising that many of the short periods reported by ASAS-SN are longer aliases of the periods we find. It is encouraging that source confusion does not appear to be a factor in the overwhelming majority of cases.

4.5. Interpretation of Periods

Periodic behavior in stars can have different origins and interpretations, and the shape of the LC or the periodogram can shed light on the mechanism. Older clusters (Pleiades and Praesepe) have less diversity of LC shapes than younger clusters (USco, ρ Oph, Taurus, Taurus Foreground); this is a result of circumstellar disks (both accretion from and occultation by disks). UCL/LCC is not as old as the Pleiades, but it is older than USco. Thus, we find LCs covering the full range of types identified in our earlier papers (Papers I-VI). Here we briefly summarize the physical interpretation of the observed LCs. Table 1 collects all the counts and sample fractions.

4.5.1. The Straightforward Rotators

About 90% of the members are periodic (see Table 1). Of those, $>60\%$ of the stars are sinusoidal periods, or close to sinusoidal periods. These are all consistent with variations due to a star spot on the surface, rotating into and out of view. Some stars have >1 period, though we use the first period reported in most of this analysis. We find all the same types of rotational variables as in Papers I-VI (see Table 1). The categories are: single period (one spot or group rotating into and out of view), multi-period (more than one spot or group rotating into and out of view, or binary (or higher-order multiple) each with a spot/spot group rotating into and out of view), double-dip (two spots/spot groups rotating into and out of view), moving double-dip (two spots/spot groups rotating into and out of view that are moving/evolving with respect to each other and/or latitudinal differential rotation), shape changers (spot/spot group evolution and/or latitudinal differential rotation), beaters (>1 close P ; multiple stars or latitudinal differential rotation), complex peak (spot/spot group evolution and/or latitudinal differential rotation), resolved close peaks (>1 close P ; multiple stars or latitudinal differential rotation, or source confusion), and resolved distant peaks (>1 very different P ; multiple stars or source confusion).

Separately, there are pulsators, typically manifesting as a forest of very short periods, but in the case of *TESS* can also manifest as just a very short period. In our *K2* work, we found in many cases that the strongest peak of those pulsators is likely closely related to rotation, based on where such stars fall in the P vs. color diagrams. We also have five stars with phased LCs that resemble those of RR Lyr stars, but at significantly faster periods; we have identified them as possible pulsators. In the present analysis, we have left the pulsation periods in the sample, but removed them from the plots. They are listed in Appendix C.

The sample fractions and numbers for these LC types in UCL/LCC are in Table 1, which could be compared to Table 3 in paper VI which includes the same analysis for all the clusters in papers I-VI. Direct comparison is somewhat complicated, however. With more than 3500 member stars, the UCL/LCC member sample has more than 3 times as

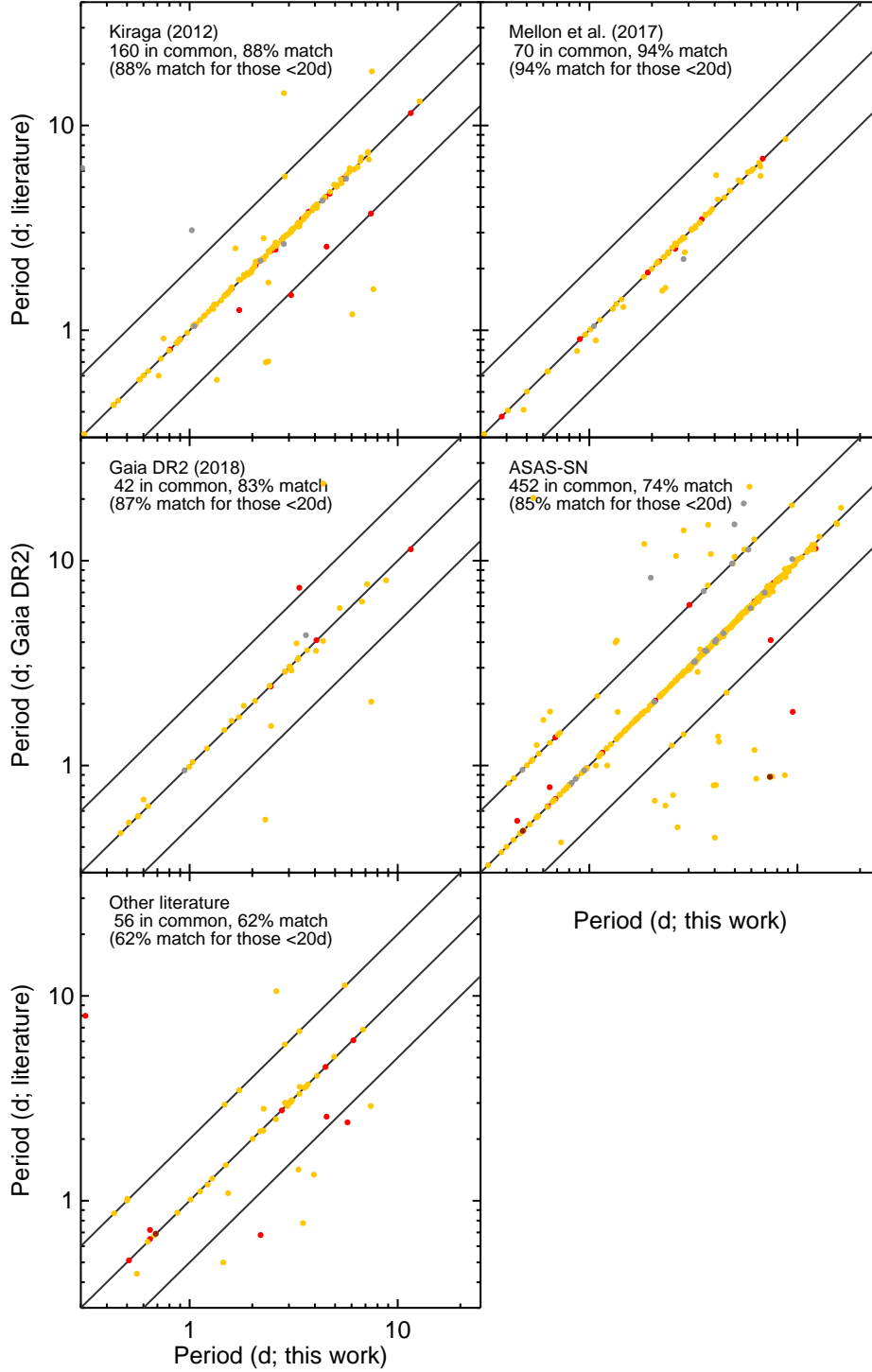


Figure 8. Comparison of periods derived here with those found in the literature. Upper left: Kiraga (2012) periods; upper right: Mellon et al. (2017) periods; center left: Gaia DR2 periods; center right: ASAS-SN periods; lower left: all other literature (see text and Table 4). Periods >20 days not shown. In all panels, gold, silver, and bronze members are indicated, along with discarded sources (red); note that some of the discarded sources are rejected because the period in the LC cannot be securely tied to an individual source. Most periods agree well; percentages quoted in figure indicate those periods matching within 20%, overall and just for those periods reported in the literature to be <20 days. Note that most points in these plots fall on the 1:1 line.

many stars as in our USco member sample, more than 4 times as many as in our Pleiades member sample, and more than 20 times as many as in Taurus or ρ Oph. With the various issues affecting the periods we can find using *TESS* data (see Sec. 4.2), it may not be fair to compare, e.g., the fraction of multi-period stars between *TESS* and *K2*, or the fraction of stars that are shape changers, when the noise characteristics of *TESS* are so different than *K2*. Overall, the fraction of periodic stars is in line with what we expect for a situation where some of the stars have circumstellar disks. Detailed comparison beyond that may not be easily possible until we have more experience with *TESS* data, more specifically understanding the noise characteristics enough to know if we are incorrectly categorizing some of the *TESS* LCs using the classes developed with *K2* data.

4.5.2. The More Complex Rotators

Stauffer et al. (2017) discussed stars then identified as scallop shells, flux dips, and transient flux dips. These unusual LCs have sharp, angular features in the *phased LC*, that are too broad for planets, and too small for spots. Most such sources are fast-rotating, disk-free M stars. We interpreted these LCs as due to matter entrained in coronal loops (Stauffer et al. 2017). Stauffer et al. (2018) found more, as did Zhan et al. (2019), Bouma et al. (2020), and Günther et al. (2022).

Stauffer et al. (2021) identified ~ 30 such objects in UCL/LCC, based on early explorations of the data we present here. After a more complete analysis, we find ~ 100 stars total (~ 70 new) in this LC category (see Table 1 and Appendix C). Due largely to lower signal-to-noise in the LCs, some of these new candidates may not be as unambiguously identifiable as the scallop shells/flux dips in Stauffer et al. (2021). While most of the scallop shells/flux dip LCs can be linked to specific stars, unfortunately, two of the stars from Stauffer et al. (2021) are identified here as clearly confused with other sources (TIC 89026133 and 89026136; see Sec. 4.2 and Appendix C). Several other targets having these kinds of LCs are also currently impossible to link to specific stars. Secure identification of exactly which star is creating the patterns awaits a later investigation.

The fact that we have ~ 100 stars in this LC category is not surprising. The previous literature has shown that these LCs occur more frequently in younger clusters. Fractionally, we have found them to be $\sim 1\%$ of the Pleiades sample, $\sim 3\%$ of the USco sample, and $\sim 4\%$ of the Taurus sample, so it is not at all surprising to find $\sim 3\%$ among our UCL/LCC sample; the fraction is consistent with the discovery rate in other young clusters studied with *K2*.

Stauffer et al. (2021) also identified a star described there as having “icicle-like” features in the LC, arising from a beating between the intrinsic period (where the shape of the LC involves a dip) and the *TESS* sampling rate. In that case, it was a photometric binary with two periods. Now, with the larger member sample, there are a few more LCs exhibiting this broad characteristic, some of which have only one period and few of which are obviously binaries. We have simply identified them as being periodic at the appropriate period. Some of the “icicle” stars have dips suggestive of eclipsing binaries.

There are many obvious eclipsing binary LCs among the UCL/LCC stars, and some additional LCs that could be eclipsing binaries or could be flux dips. Of the eclipsing binaries, in some cases, we can omit the eclipses and still derive a rotation period from the photospheric component of the LC. We have listed the P_{rot} in the tables (and used those in the plots). In Appendix C we have listed the eclipsing binaries (and candidates) along with the P_{binary} where we can derive it.

We tabulate ‘timescales’ for LCs with repeating patterns that are probably not rotation periods in Appendix D.

4.5.3. The Disk-Influenced Periodic Patterns

Some stars in UCL/LCC still retain their disks, and they exhibit LC types associated with circumstellar material, namely dippers and bursters (see, e.g., Cody et al. 2014; Cody & Hillenbrand 2018; Cody et al. 2022). These sources have a “continuum” LC that is punctuated by dips (fading) or bursts (brightening). Dippers are interpreted as occultations by disk material, while bursters are interpreted as accretion impacts. These stars all have large IR excesses.

Note that the LCs identified as being bursters or dippers are identified as such without reference to the SED; they all turn out to be disked, however, based on the SED.

Tajiri et al. (2020) also identify dippers from *TESS* full-frame images. Among their sample, we independently identified TIC 226241509, 243324939, 266079454, 334999132, & 412308868 as dippers in this work.

4.6. Range of Periods

In addition to the brightness and faintness limits imposed by *TESS* data availability, we are limited by *TESS* cadence in the range of P to which we are sensitive. The shortest reliable period that we have identified is 0.436 days (=1.05 hrs); the longest is 17.1 days. Our range of identified periods is comparable to the range we expect for stars with ages similar to the UCL/LCC clusters.

Our approach to finding periods in the *TESS* data has to include star-by-star inspection and refinement after initial automatic processing, despite the potential for biases introduced by this human-based process. It enables us to easily find targets subject to obvious source confusion (Sec. 4.2). There are enough very large outliers in the LCs, and a suspiciously common ~ 6 -7 day period (which we suspect is instrumental or introduced by LC extraction), that the investment of time per star is well-spent. Given the comparison to the literature, we suspect that we may have conservatively dropped some legitimate ~ 6 -7 day periods. While no one else in the literature to our knowledge has reported problems with ~ 6 -7 day periods, others have reported difficulty with $P > 27$ days (see, e.g., Avallone et al. 2022, and references therein); we don't have any periods that long.

It can be harder to obtain rotation periods for disked stars as a result of stochastic contributions from the disk and/or accretion (see e.g., Cody & Hillenbrand 2018 and references therein). Among all the disked stars, the periodic fraction is $\sim 85\%$, to be compared with $\sim 90\%$ of the non-disked stars (Table 1). Thus, our periodic member sample is likely biased against disked stars for astrophysical reasons.

5. UCL/LCC COLOR-MAGNITUDE AND PERIOD-COLOR DIAGRAMS

In this section, we present the UCL/LCC sample in the Gaia-based absolute color-magnitude diagram (Sec. 5.1), in the K_s vs. $(V - K_s)_0$ observed color-magnitude diagram (Sec. 5.2), and in the period vs. $(V - K_s)_0$ diagram (Sec. 5.3). In each case, we discuss how the subsamples are similar or different in these diagrams.

5.1. Gaia Color-Magnitude Diagrams

Figure 9 presents absolute Gaia color-magnitude diagrams for the three member samples (gold, silver, and bronze) and the rejected sample. The stars that appear to be significantly above the zero-age main sequence (ZAMS) or near-ZAMS, as defined by the rest of the sample, are immediately apparent; these are candidate giants or other non-members. Our gold sample is defined to have none of these stars included. A significant fraction of the silver members (Table 1 and Fig. 9) have as the one mark against them only a discrepant Bailer-Jones distance.

At first glance, the ZAMS in all of the member subsamples (gold, silver, bronze) looks similar. Omitting all of the giants and using a 2-dimensional 2-sided KS test in addition to histograms of color or absolute G , we can compare member subsamples in more detail. The gold sample has, by far, the most well-populated early ZAMS, down to about $G_{BP} - G_{RP} < \sim 2$ (and $M_G \sim 7$), such that it is still significantly different from the other subsamples, even after omitting the giants. This makes sense, as the brighter stars will be easier to measure and should therefore be easier to identify as secure members. The silver and bronze subsamples are most similar to each other, with fractionally more fainter stars than the other subsamples near $G_{BP} - G_{RP} < \sim 3.2$.

As in Fig. 9, the JHK_s diagrams presented above in Fig. 3 also suggested that all the member subsamples are similar. In detail, though, the gold sample has more early-type stars, making it different at a statistically significant level, while silver and bronze are the most similar.

5.2. V and K_s Color-Magnitude Diagrams

Fig. 9 shows a tightly constrained empirical ZAMS, but Gaia data are not available for most of the stars in the other clusters in Papers I-VI. Papers I-VI used $(V - K_s)_0$ as a proxy for mass, and to facilitate the comparisons we wish to make here, we employ $(V - K_s)_0$ colors for UCL/LCC as well, over the readily available and reliable Gaia colors.

Figure 10 shows the observed (not absolute) K_{s0} vs. $(V - K_s)_0$ diagrams for our UCL/LCC member sample, revealing a cluster locus that is broader than expected given Fig. 9. A significant contributor to the scatter in Fig. 10 comes from variations in distance across UCL/LCC members. The gold sample spans the entire range of $(V - K_s)_0$ colors, and the M stars are particularly well-populated. The silver and bronze samples do not span the full range of $(V - K_s)_0$, and have fractionally fewer M stars. Nearly all the stars are periodic (Table 2). Fig. 10 also reveals that there is more scatter in the rejected targets than the other subsamples, which makes sense particularly if there is source confusion even in 2MASS.

5.3. Period-Color Diagrams

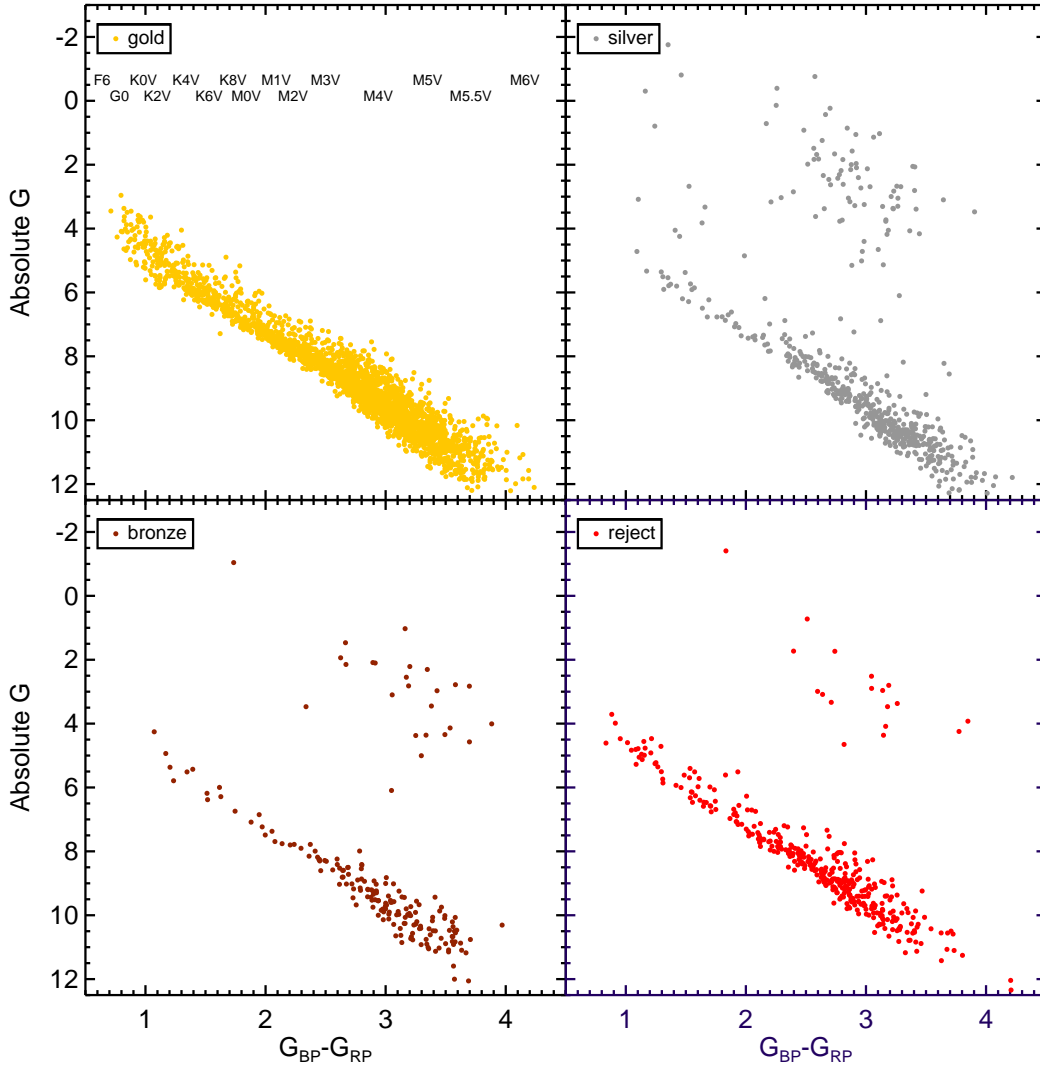


Figure 9. Absolute Gaia color-magnitude diagram, using distances from Bailer-Jones et al. (2018) for the gold, silver, and bronze members, and the rejected targets (see Sec. 2.3). The stars that appear to be giants (or even just significantly above the ZAMS defined by the rest of the sample) are immediately apparent. The gold member sample, by definition, has no objects with Bailer-Jones distances > 300 pc.

Figure 11 shows the P vs. $(V - K_s)_0$ plot for the members and rejected targets in UCL/LCC. Both the P and $(V - K_s)_0$ values are listed in Table 2 (or Table 3 for the rejected targets). As in our *K2* rotation papers, for stars with more than one period, we have taken the first period and the identified $(V - K_s)_0$ as representative of the same star (likely the primary if it is a multiple).

The gold sample has clear structure in P vs. $(V - K_s)_0$. Most of the M stars are organized into a sequence of steeply increasing rotation rate (decreasing periods) going from early M through at least M4/M5. The higher mass stars (G and K spectral types) have considerable scatter, but they seem to be, on average, more slowly rotating than most of the M stars, with the Gs also rotating much faster than the Ks. The bronze and silver distributions seem to have similar structure, but there are too few stars to define it clearly. It is unsurprising that the rejected stars have the most scatter, since it is less likely here that the measured P goes with the assumed $(V - K_s)_0$.

Anticipating discussion later in the paper, the scatter found in Fig. 11 is substantial, even for the gold sample. In other clusters, any scatter had been a result of reddening corrections or unresolved binaries. Reddening corrections

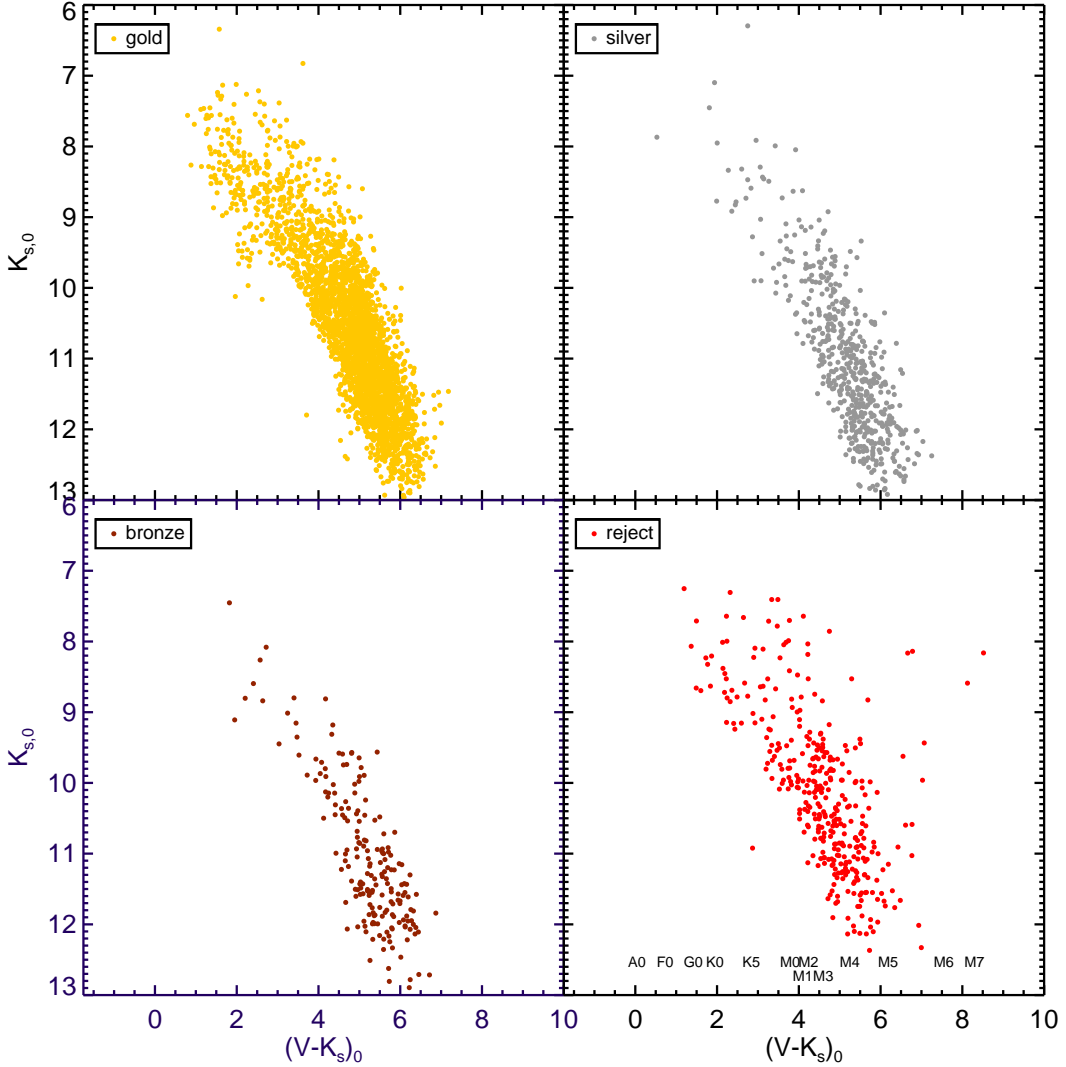


Figure 10. Dereddened K_s vs. $(V - K_s)_0$ for the gold, silver, and bronze members, and the rejected targets. The gold sample is the most well-populated across the full color range. There is more scatter here in all member subsamples than in Fig. 9, in part because the stellar distances vary significantly over the cluster. The discarded sample has the most scatter, which makes sense given that source confusion is important for many of the rejected stars.

are not as big a concern in UCL/LCC (Sec. 3.3). There is not enough literature for us to constrain significantly the binary fraction among our UCL/LCC member sample, though any such binaries would have had to survive the culling based on accurate Gaia measurements, which is likely to omit binaries.

If we look at the fraction of stars that have more than one period, as a function of location in the P vs. $(V - K_s)_0$ plot, the multi-period fraction rises steeply on the edges of the structure traced by the bulk of the points. With *TESS*, especially given the relative apparent difficulty of finding multiple periods (Sec. 4.3), without additional data, we cannot be sure that the outliers in P vs. $(V - K_s)_0$ are photometric binaries, or instead primarily a result of source confusion affecting the P attributed to a given star. Given the likely bias against binaries from Gaia, we have to suspect that source confusion is a factor.

As the UCL/LCC sample is large, and there is some evidence for variation of stellar ages across the association, we explored whether or not there is any evidence for changes in the distribution of P vs. color across the sky in various member subsamples. We did not find any evidence for this.

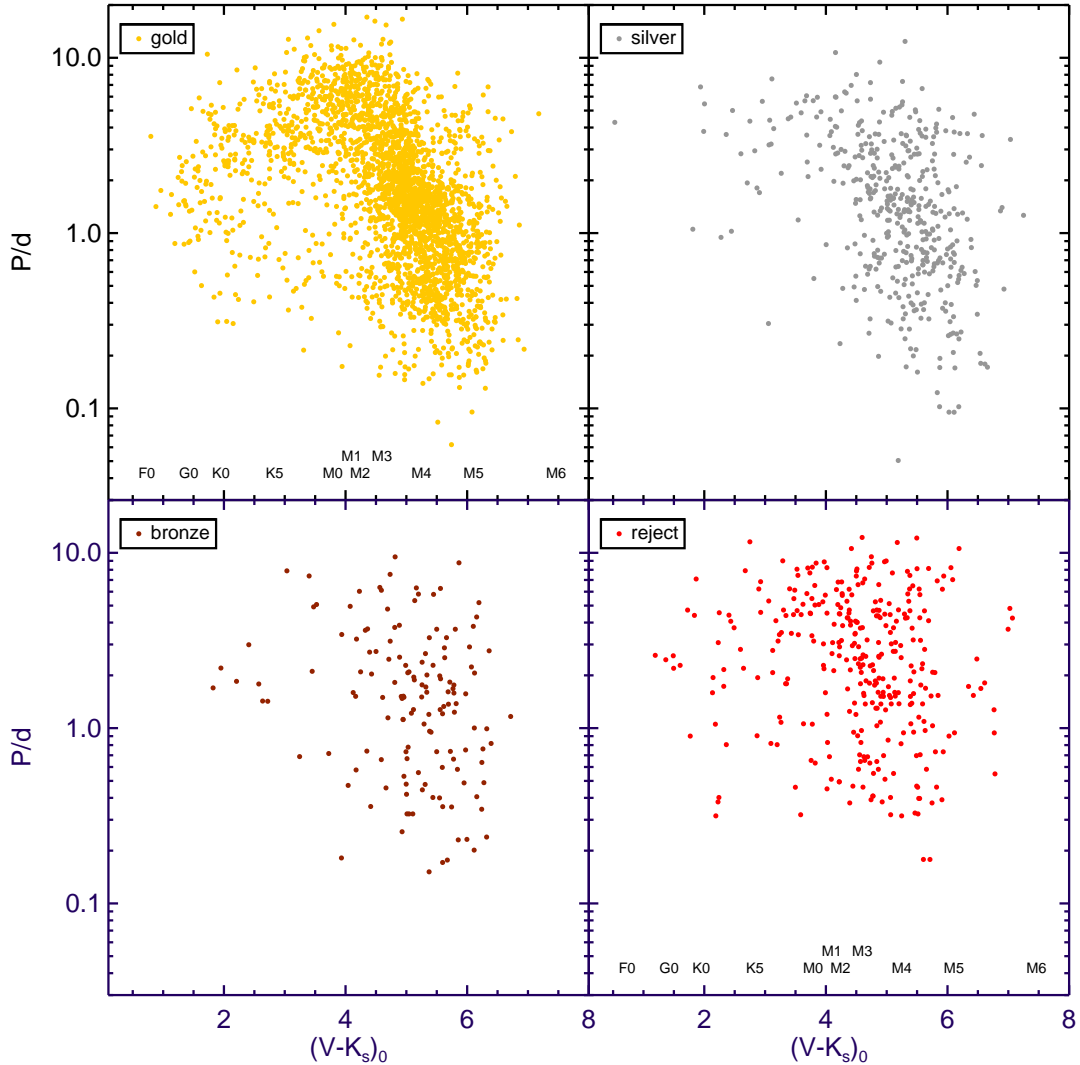


Figure 11. P (in days) vs. $(V - K_s)_0$ for the gold, silver, and bronze members, and the rejected targets. Note that there are two stars from the discarded sample with $(V - K_s)_0 > 8$, beyond the plot limits. The gold sample is the best populated and it is easiest to see structure in this distribution. The structure is similar to that found in other clusters; see the text and Fig. 12.

6. PERIOD-COLOR DISTRIBUTION IN CONTEXT WITH OTHER CLUSTERS

In this section, we put UCL/LCC in context with the other clusters we have studied with $K2$ data. We assume that the stars in UCL/LCC represent snapshots in time of the same population as found in the other clusters (c.f., Coker et al. 2016). We note as well that the rotation evolution is likely influenced by the local UV environment (see Roquette et al. 2021), which would matter locally if the high-mass stars in UCL/LCC have influenced local star evolution. We first compare the entire distribution of UCL/LCC to well-populated clusters (Sec. 6.1), then narrow down to consider just the disk-free M stars in those clusters (Sec. 6.2). Next, we put UCL/LCC in context with rotation rates from 8 other clusters studied with $K2$ (Sec. 6.3), some very sparsely populated. Finally, we consider the influence of disks, particularly among the M stars (Sec. 6.4).

6.1. Comparing to Well-Populated Clusters

The period-color structure in UCL/LCC that is most obvious in the gold sample is suggestive of something intermediate between the distribution in USco (Paper V) at ~ 8 Myr and the Pleiades (Paper I) at ~ 125 Myr, which is

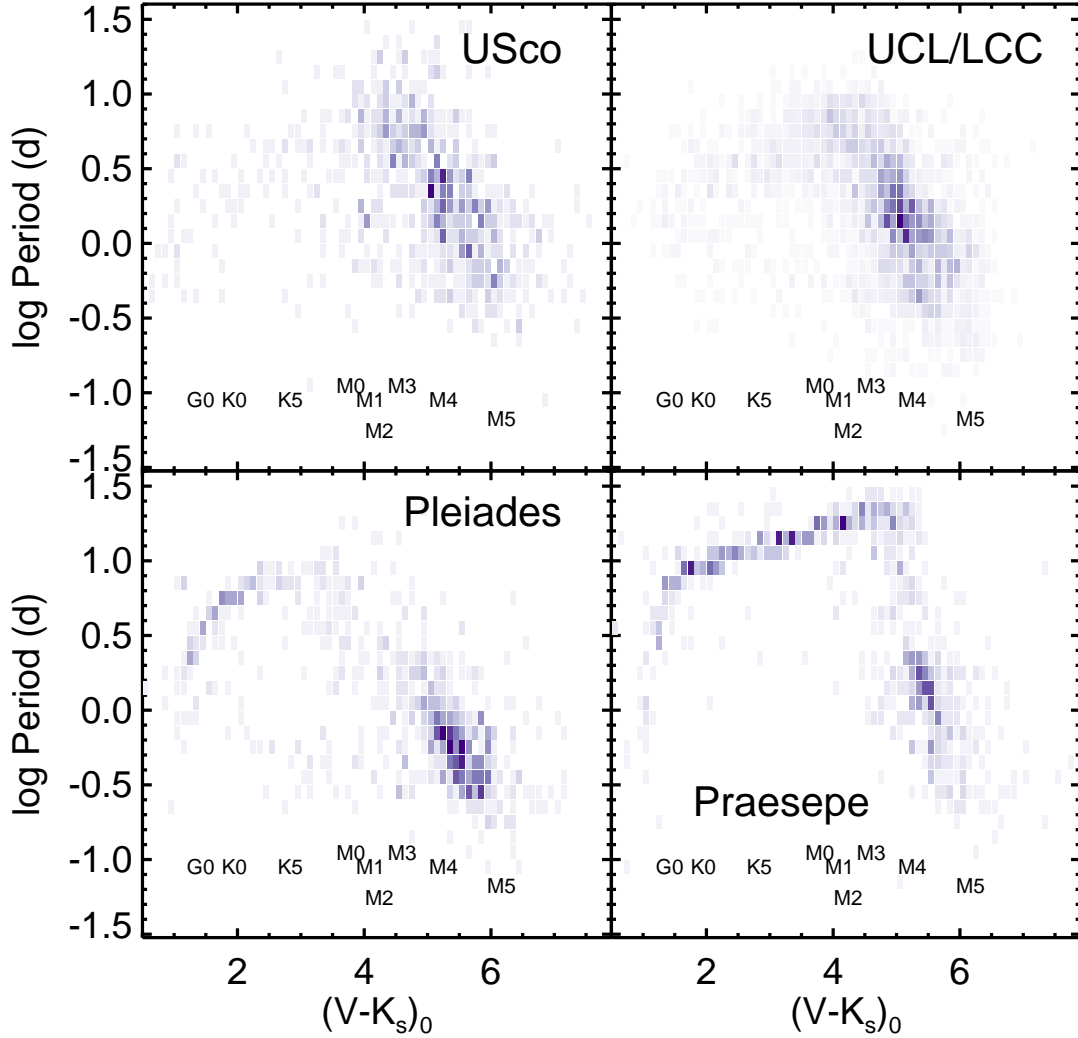


Figure 12. P (in days) vs. $(V - K_s)_0$, disks removed: density map, where darker shades indicates more sources in that cell. Each cluster is self-normalized such that the darkest shade is the best populated within that cluster, which is a different absolute number (and sample fraction) in each cluster. On the high-mass end, the distribution is well-defined in Pleiades and Praesepe, but far less so in USco or UCL/LCC (which is just the gold member sample). The low-mass end is well-defined in all four clusters. See the text for much more discussion.

consistent with the accepted age of UCL/LCC of ~ 16 Myr. Figure 12 shows UCL/LCC (just the gold member sample) in context with the most well-populated clusters that we have studied using *K2*: USco, Pleiades, and Praesepe (Paper IV; 790 Myr). In this plot, all the disks (secure and possible) have been removed from USco and UCL/LCC, leaving just the disk-free stars. The density map shows where sources are clustered more tightly; there are so many stars, especially in UCL/LCC, that it is hard to appreciate the point density if only individual points are plotted.

The distribution for the G and K spectral types that is very obvious and well-defined by the Pleiades age is far less obvious in the younger UCL/LCC, and even less obvious in the younger yet USco cluster. In Paper V, we suspected that the reddening in USco, which is patchy and sometimes large, meant the uncertainties in the reddening correction added artificial “smearing” to the distribution, rendering the higher masses appearing to be less organized. However, in UCL/LCC, there is far less reddening, and less patchy reddening (Sec. 3.3 and Fig. 3), yet the early-type “branch” is still not anywhere near as organized as in the Pleiades. The most extreme outliers in UCL/LCC may be subject to

source confusion (Sec. 5.3), but much of this ‘disorganization’ may be a real feature of this rotation distribution for G and K spectral types in clusters $\lesssim 20$ Myr old.

6.2. Comparing the M Stars in the Well-Populated Clusters

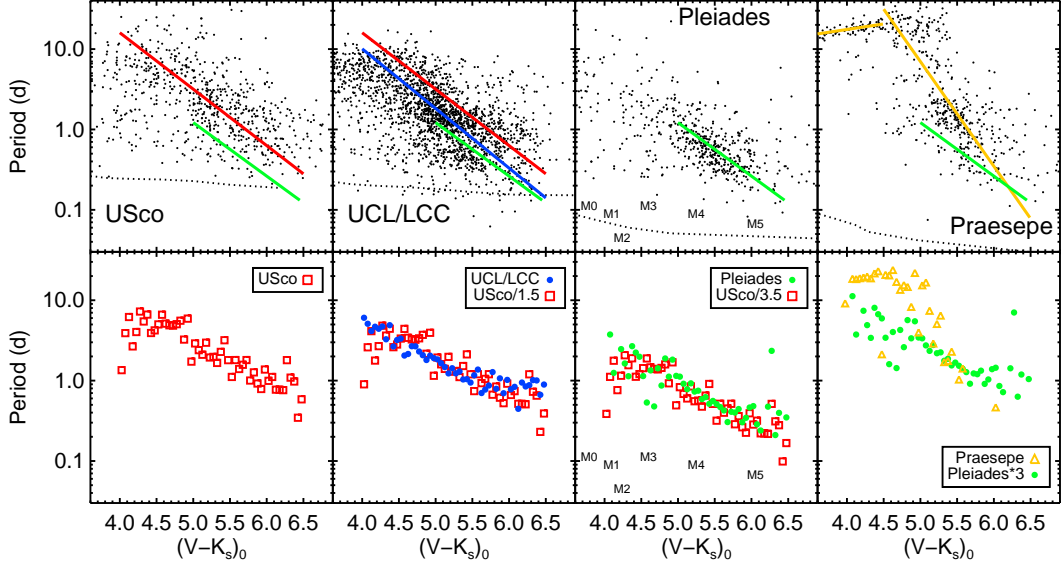


Figure 13. P (in days) vs. $(V - K_s)_0$ for M stars, disks (high-confidence and possible) removed, and just UCL/LCC gold members. Top row: observations (breakup is dotted line); Bottom row: medians of observations in $(V - K_s)_0$ bins. Column 1: USco; Column 2: UCL/LCC; Column 3: Pleiades; Column 4: Praesepe. In top row: USco fit: red line; UCL/LCC fit: blue line; Pleiades fit: green line; Praesepe fit: yellow line. In bottom row: USco binned data: red symbols; UCL/LCC binned data: blue symbols; Pleiades binned data: green symbols; Praesepe binned data: yellow symbols. USco binned data are shifted in second panel to match UCL/LCC, and shifted in third panel to match Pleiades. Pleiades is shifted in fourth panel to attempt to match Praesepe. UCL/LCC fits neatly in between USco and Pleiades, with a slope that is indistinguishably the same.

Most of the stars in the present analysis are M stars, and Figure 13 highlights their behavior across the clusters. Again, disks have been removed from USco and UCL/LCC, so these are just the disk-free, gold member M stars. The top row has a linear fit to the M stars and the bottom row includes running medians and scaled running medians. Paper V pointed out that the M star slope between USco and Pleiades is the same, just shifted as the stars contract onto the main sequence. UCL/LCC fits neatly in between USco and Pleiades, with a slope that is indistinguishably the same. The slope for USco/UCL-LCC/Pleiades is vastly different than the slope for Praesepe, which makes sense since the M stars are spinning up through the Pleiades, and spinning down by the older age of Praesepe, likely incorporating wind braking (Paper V).

In both Figs. 12 and 13, particularly for UCL/LCC, it is apparent that there is a denser region of points near $(V - K_s)_0 \sim 5$ mag, $\log P \sim 0.15$ ($P \sim 1.4$ days). This dense peak is very obvious in UCL/LCC and far less prominent in the other clusters. In USco, the distribution is more diffuse, and the peak occurs at the same $(V - K_s)_0$, but slightly slower, $\log P \sim 0.35$ ($P \sim 2.2$ days). For the Pleiades, the distribution is elongated along the entire distribution of M stars, but the peak is much redder and faster, at $(V - K_s)_0 \sim 5.55$, $\log P \sim -0.25$ ($P \sim 0.56$ days). The Praesepe M stars have an entirely different distribution. The M star peak is actually up on the slow branch, at $(V - K_s)_0 \sim 4.15$, $\log P \sim 1.25$ ($P \sim 17$ days); removing the slow branch, the peak is at the same color as the Pleiades, $(V - K_s)_0 \sim 5.55$, and about the same period as UCL/LCC, $\log P \sim 0.15$ ($P \sim 1.4$ days).

There are several stars with very fast periods, apparently faster than breakup in some cases; they are found in all of the member subclasses, and some appear to have IR excesses. Those LCs, and their periods, appear legitimate and unambiguous, leading us to conclude that perhaps something may be wrong with the linkage between the LC and the stellar source. In cases where the apparent IR excess originates in a single band at WISE-3 or WISE-4, the possibility exists that the relatively low-spatial-resolution of WISE is also subject to source confusion, so neither the P nor the

IR excess may be correctly tied to the star associated with the $(V - K_s)_0$; further exploration of these cases, with higher spatial resolution data, is needed.

6.3. Comparing to Other Clusters

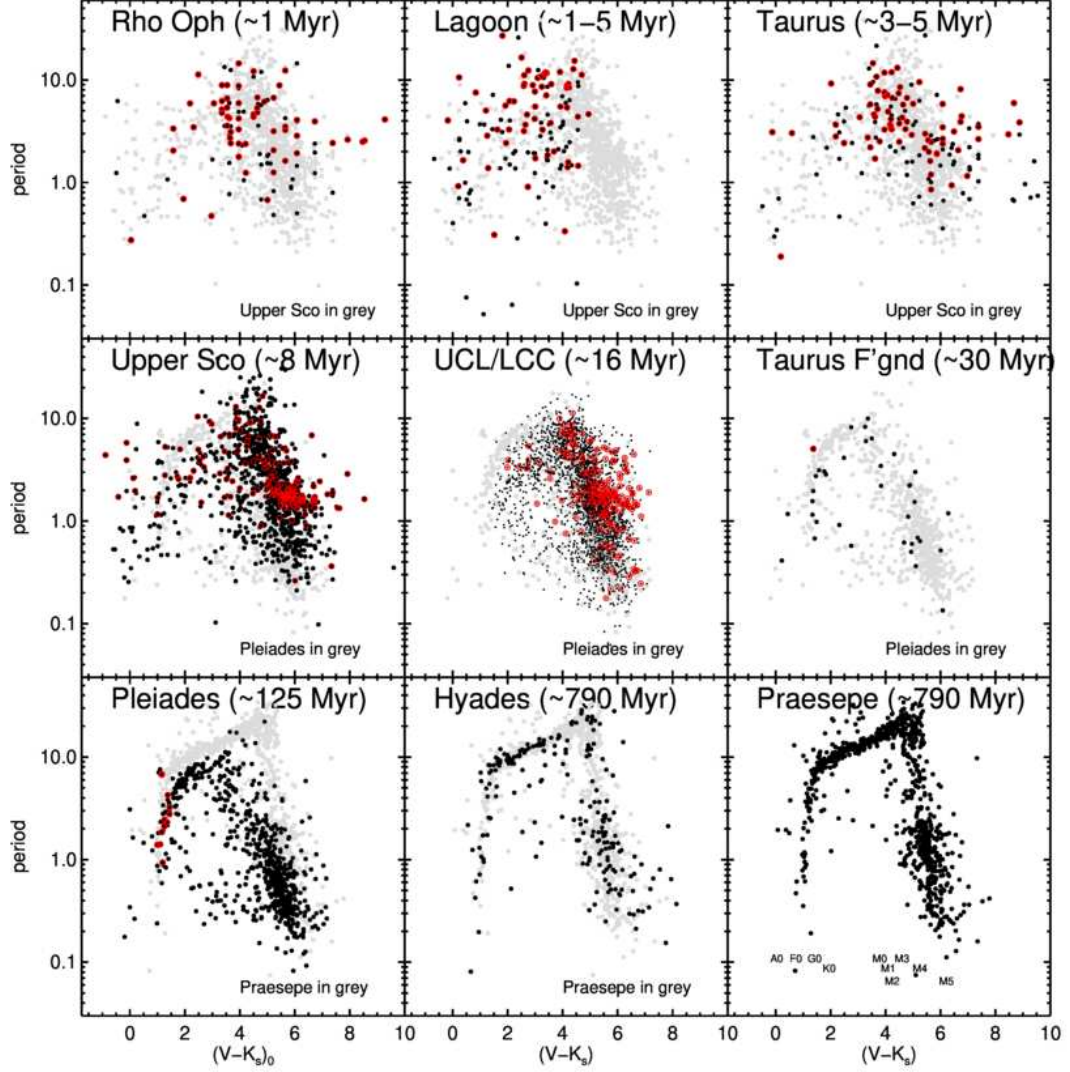


Figure 14. P (in days) vs. $(V - K_s)_0$ for all stars in 9 clusters, all except UCL/LCC from $K2$. Stars with IR excesses (e.g., disks) are shown with an additional red circle. The first row has the youngest most populous cluster, USco, underplotted in grey. The second row has the Pleiades underplotted in grey. The third row has Praesepe underplotted in grey. The points are smaller for UCL/LCC because there are so many points it is hard to see the patterns otherwise. UCL/LCC points are all from the gold member sample. It again seems to fit well “in sequence” with the other clusters around it. References for data: Rho Oph: Paper V; Lagoon: Rebull et al. (in prep); Taurus: Paper VI; USco: Paper V; UCL/LCC: this work; Taurus Foreground: Paper VI; Pleiades: Papers I & II; Hyades: Rebull et al. (in prep); Praesepe: Paper IV.

Fig. 14 shows the data from UCL/LCC in context with all the other space-based rotation rates from $K2$ from our prior work. For each cluster, an older well-populated cluster is underplotted to guide the eye regarding the evolutionary patterns. The UCL/LCC distribution is in the middle of the evolutionary age sequence. The structure in the Hyades is indistinguishable from that in Praesepe. In the case of the Taurus Foreground, there are so few stars that it is hard to identify any structure unique to that cluster. At the youngest ages, determining the structure is greatly complicated

by the uncertainties added by the “smearing” imposed by reddening corrections and contributions from disk excesses. The structure seen in USco is vaguely apparent in Rho Oph, Lagoon, and Taurus. In the case of the Lagoon, limited sensitivity complicates interpretation at the lower masses.

In all of the three youngest clusters, there are relatively few stars, there is additional smearing due to reddening corrections, and there is a substantial disk fraction. The disks appear to affect the rotation distribution. Most notably there is an obvious ~ 2 day pileup of disks in USco as well as in UCL/LCC. We investigate the influence of disks in the next subsection.

6.4. Disks and Rotation

Figure 15 shows where the disks are on the sky, using the same orientation and units as Fig. 1, but with different interpretation of the point color. Disks in USco are as in Paper VI; high-confidence and lower-confidence disks in UCL/LCC are identified here and comprise $\sim 7\text{-}8\%$ of the sample. There are obvious clumps of stars with disks, but little large-scale systematic structure. There is also no obvious systematic difference (in distribution or in disk fraction) between UCL and LCC; given their similarity in ages, this is not surprising.

There is a theoretical expectation that primordial disks lock the rotation rate of the star to that of the inner disk (e.g., Ghosh & Lamb 1977; Königl 1991). When the disk disperses, which is thought to happen at about the age of UCL/LCC for M stars, the star is free to spin up. We thus now explore the relationship between disks and rotation for the M stars in UCL/LCC.

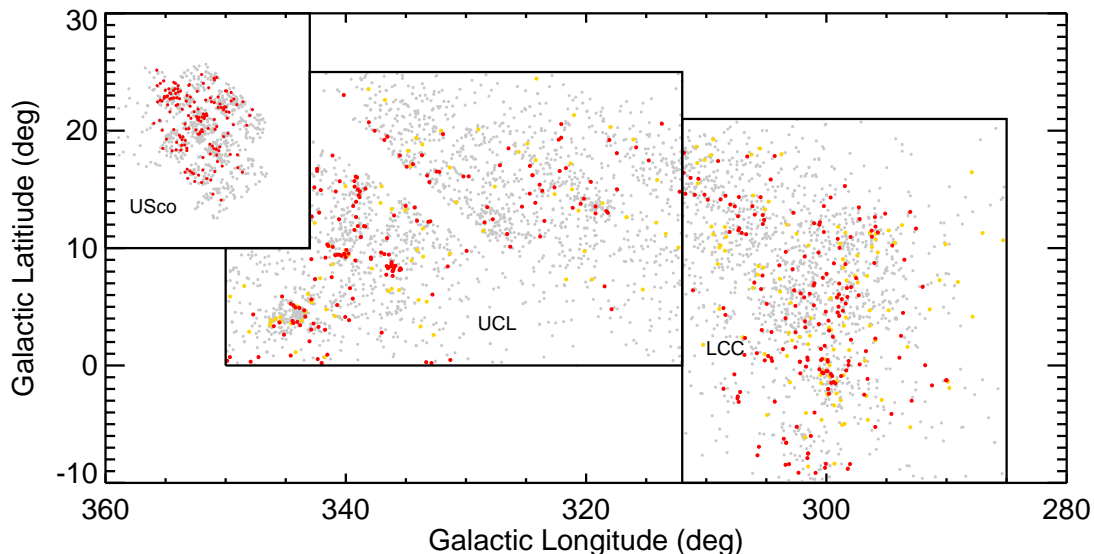


Figure 15. Location of targets in Galactic coordinates, as in Fig. 1. Stars with high-confidence disks from UCL/LCC (or USco; paper IV) are red points; stars with lower-confidence disks from UCL/LCC are yellow points. Grey points are simply stars with LCs. The high-confidence disks are clustered, but not nearly as much as they were in USco. The high-confidence disk fraction in both UCL and LCC is $\sim 7\text{-}8\%$, and there is no obvious large-scale gradient in disk fraction with position among UCL/LCC.

Figure 16 zooms in on the M stars in the P vs. $(V - K_s)_0$ plot for USco, the confident UCL/LCC disks, and the possible UCL/LCC disks. As discussed in detail in Paper V, the USco plot has a clear pileup of disked stars at ~ 2 days, which we believe to be a signature of disk locking. For the confident disks in UCL/LCC (middle panel), there is a similar very obvious ~ 2 day pileup in the mid-M stars. Using a 2-dimensional 2-sided KS test, the disked and non-disked samples are statistically significantly different from each other in the first two panels of Figure 16.

Few disked M stars are found to rotate faster than ~ 2 days in USco (first panel; only 3% of the disked stars have $P < 1$ day, compared to 26% of the non-disked). However, there are more disked stars rotating faster than ~ 2 days in UCL/LCC (middle panel; 20% of the disked stars have $P < 1$ day, compared to 32% of the non-disked). It is not immediately obvious why this would be the case. Since source confusion is an important concern, this is perhaps the most likely reason, meaning largely TESS confusion, but also possibly confusion in WISE. These stars could be fast

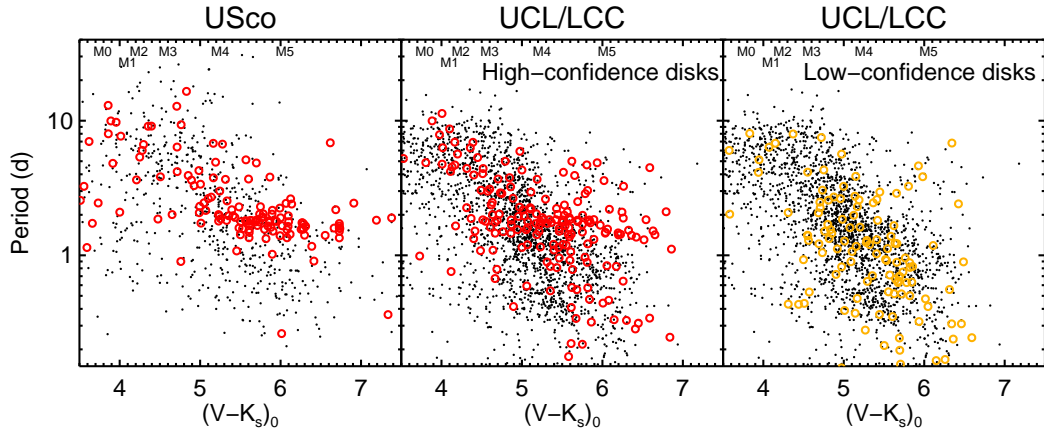


Figure 16. P (in days) vs. $(V - K_s)_0$ for M stars from the gold member sample, where a black point is a disk-free M star, a red circle is a high-confidence disked M star, and a yellow circle is a lower-confidence disked M star. The left panel is USco, and the other two panels are UCL/LCC (the black dots are the same in the middle and right panels). The disked stars have an obvious “pile-up” near 2 days among the M stars, and there may be a slope to that 2-day pile-up; see the text. The lack of structure in the last panel reinforces our lack of confidence in those disks in general.

rotating because they are binaries, but they do not appear to be photometric binaries in an optical color-magnitude diagram, nor are they in general those stars with multiple periods (in $K2$, we found that in particular, M stars with multiple periods were also often photometric binaries).

Figure 17 shows the WISE IR excess $([3.4] - [12])_{\text{observed}} - ([3.4] - [12])_{\text{expected}}$ as a function of P for bins in $(V - K_s)_0$. It is straightforward to see that the fast rotating disked stars do not, in general, have multiple periods, nor are they the stars with the larger $12 \mu\text{m}$ IR excesses. A handful of these stars do have secondary periods that are >1 day, or have discarded periods that are >1 day. Follow-up observations of these targets are warranted. It is still the case, as it is for USco, that UCL/LCC stars with disks tend to rotate slower than the ensemble. Alternately, fast rotating stars tend not to have disks.

There are enough stars in this UCL/LCC member sample that we can break down the distribution into relatively fine bins of $(V - K_s)_0$, and investigate a relationship that was hinted at in USco. In Fig. 16, in both USco and UCL/LCC, the pileup at $(V - K_s)_0 \sim 5-6$ and ~ 2 days seems to have a downward slope. Fig. 17 attempts to explore this further; for stars with $(V - K_s)_0 > 4.5$, it shows the mean P calculated for disked stars with $([3.4] - [12])_{\text{observed}} - ([3.4] - [12])_{\text{expected}} > 0.3$ in each panel. The M3 stars have a mean P near 2.5 days, and the M5 stars are near 1.5 days, suggesting that among the disked stars with large IR excesses, less massive stars are rotating faster.

The discussion with Fig. 12 above noted that the distribution of disk-free UCL/LCC M stars was very sharply peaked at $P \sim 1.5\text{d}$, which is quite close to the pileup of the M star disked stars at $\sim 1.5-1.8$ days. We speculate whether this clump consists of stars that have relatively recently shed their dust disks and therefore unlocked from their disk, but have not yet had the time to spin up in response, a process that may take a few million years (e.g., Roquette et al. 2021).

We note that the last panel in Fig. 16 has very little structure reminiscent of any of the structure seen in the other panels, reinforcing our lack of confidence in those stars having believable disks.

7. SUMMARY AND CONCLUSIONS

We have presented space-based spot-modulated rotation rates from *TESS* for $\sim 90\%$ of ~ 3700 UCL/LCC members ($\sim 91\%$ of the ~ 3000 most likely members).

We started from a set of members assembled in the literature largely from Gaia DR2 analyses. We winnowed down the sample based on what supporting data we could find, whether or not we could obtain a *TESS* LC, and whether or not that *TESS* LC could reliably be tied to that source. Based on the available information, we placed the stars into three member bins: gold (the overwhelming majority of the members), silver, and bronze. We also kept track of the sources rejected as members. We identified IR excesses from any available IR band, but WISE-3 ($12 \mu\text{m}$) was the most widely available band, which we used for plotting purposes.

We identified periods in the *TESS* LCs that compare well with those in the literature, up to ~ 15 days of half a *TESS* campaign duration. We find periods for $\sim 90\%$ of the UCL/LCC members, with $>60\%$ of those sinusoidal periods, or

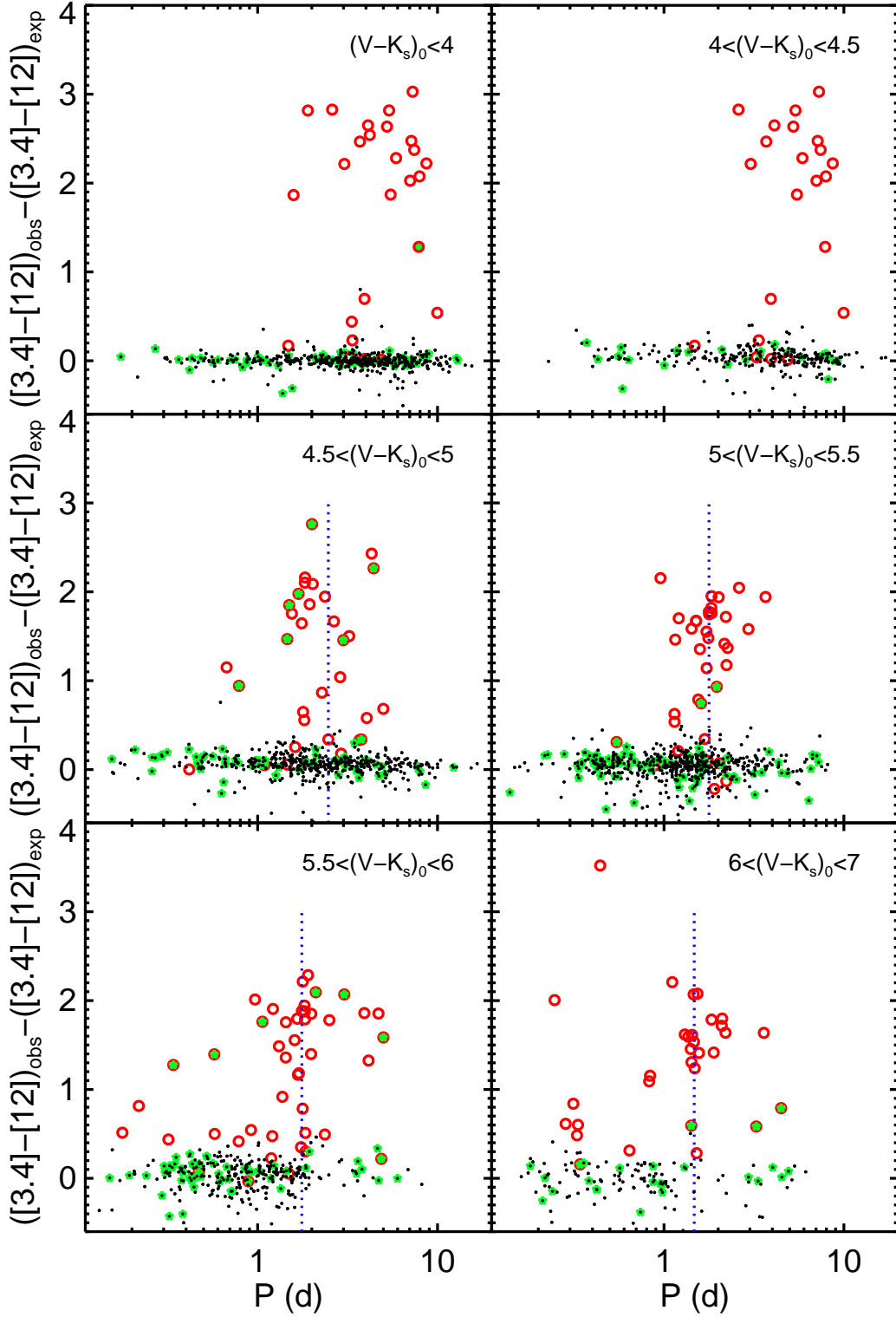


Figure 17. WISE IR excess (observed – expected $[3.4]-[12]$) for gold member stars unlikely to be pulsators, in bins of $(V - K_s)_0$, as shown in each panel. Black dots are stars without disks; red circles are stars with high-confidence disks. An additional green symbol means that there are multiple periods associated with the object, e.g., it could be a multiple or subject to source confusion. UCL/LCC stars with disks tend to be rotating slower than the ensemble, or, rather, fast rotating stars tend not to have disks. The vertical blue dotted lines in the bottom four panels is located at the mean period for disked stars with $(V - K_s)_0 > 4.5$ and $([3.4] - [12])_{\text{observed}} - ([3.4] - [12])_{\text{expected}} > 0.3$ in each panel (2.5, 1.8, 1.8, & 1.5 days). Among the disked mid-M stars with large IR excesses, M5 stars are rotating faster than M3 stars.

close to it, and interpreted as arising to spots or spot groups that rotate into and out of view. We find a similar variety of LC and periodogram types as we found in our *K2* work, but we found a lower fraction of stars with multiple periods. This could be a result of the noise characteristics of *TESS* LCs, but it could also be a result of the target selection. Most of the targets were identified based on Gaia selection, which can select against multiplicity. In our *K2* work, we found that multi-period stars, especially among the Ms, were often photometric binaries. Thus, if our input target list was biased against multiples, it makes sense that our sample is less likely to find multi-period stars. However, the noise characteristics of the *TESS* LCs are indeed very different than *K2*, so that cannot be entirely dismissed as a cause for finding fewer multi-period stars.

We find more of the scallop shells, flux dips, and transient flux dips initially identified in (Stauffer et al. 2017, 2018, 2021). Fractionally, we find them at a rate of 3% in the UCL/LCC sample, which is quite consistent, given relative ages, with 1% of the Pleiades sample, 3% of the USco sample, and 4% of the Taurus sample.

The distribution of P vs. $(V - K_s)_0$ color as a proxy for mass, reveals that UCL/LCC fits in well with evolutionary expectations, given its age. Figs. 12 and 14 both show that the highest and lowest masses probed here are among the fastest rotators; the slowest rotators are in the middle masses. The higher masses are not as ‘organized’ as they presumably will be by the Pleiades age, but at the same time, they are not as ‘disorganized’ as they presumably were at the USco age. The M stars are already well-organized, and follow the same slope as is found in both USco and the Pleiades.

The disk fraction in UCL/LCC is a few percent, and as a result, there are some disk-influenced LCs – we find both bursters and dippers among the disked stars. The disked M stars form a very obvious pile-up at about 2 days in the P vs. $(V - K_s)_0$ plot (Figs. 16 and 17), a pile-up that seems to drift slightly longer as the mass decreases. Interestingly, the distribution of disk-free M stars is also sharply peaked at ~ 2 days, at the same location as the disked stars, suggesting that perhaps these stars have just freed themselves from their disks but have not yet had the time to react yet.

Some of the data presented in this paper were obtained from the Mikulski Archive for Space Telescopes (MAST). Support for MAST for non-HST data is provided by the NASA Office of Space Science via grant NNX09AF08G and by other grants and contracts. This paper includes data collected by the *TESS* mission. Funding for the *TESS* mission is provided by the NASA Explorer Program. This research has made use of the NASA/IPAC Infrared Science Archive (IRSA), which is operated by the Jet Propulsion Laboratory, California Institute of Technology, under contract with the National Aeronautics and Space Administration. This research has made use of NASA’s Astrophysics Data System (ADS) Abstract Service, and of the SIMBAD database, operated at CDS, Strasbourg, France. This research has made use of the VizieR catalogue access tool, CDS, Strasbourg, France (DOI : 10.26093/cds/vizieR). The original description of the VizieR service was published in 2000, A&AS 143, 23. This research has made use of data products from the Two Micron All-Sky Survey (2MASS), which is a joint project of the University of Massachusetts and the Infrared Processing and Analysis Center, funded by the National Aeronautics and Space Administration and the National Science Foundation. The 2MASS data are served by the NASA/IPAC Infrared Science Archive, which is operated by the Jet Propulsion Laboratory, California Institute of Technology, under contract with the National Aeronautics and Space Administration. This publication makes use of data products from the Wide-field Infrared Survey Explorer, which is a joint project of the University of California, Los Angeles, and the Jet Propulsion Laboratory/California Institute of Technology, funded by the National Aeronautics and Space Administration.

Facility: K2, 2MASS, WISE, IRSA, Exoplanet Archive

REFERENCES

- | | |
|---|--|
| AKARI team, 2010a, AKARI/FIS All-Sky Survey Bright Source Catalogue, IRSA, doi:10.26131/IRSA180 | Alfonso-Garzón, J., Domingo, A., Mas-Hesse, J. M., et al. 2012, A&A, 548, A79. doi:10.1051/0004-6361/201220095 |
| AKARI team, 2010b, AKARI/IRC Point Source Catalogue, IRSA, doi:10.26131/IRSA181 | Avallone, E. A., Tayar, J. N., van Saders, J. L., et al. 2022, arXiv:2203.15116 |
| Akeson, R. L., Chen, X., Ciardi, D., et al. 2013, PASP, 125, 989. doi:10.1086/672273 | Bailer-Jones, C. A. L., Rybizki, J., Foesneau, M., et al. 2018, AJ, 156, 58. doi:10.3847/1538-3881/aacb21 |

- Bailer-Jones, C. A. L., Rybizki, J., Fouesneau, M., et al. 2021, *AJ*, 161, 147. doi:10.3847/1538-3881/abd806
- Batalha, C. C., Quast, G. R., Torres, C. A. O., et al. 1998, *A&AS*, 128, 561. doi:10.1051/aas:1998163
- Blaauw, A. 1964, *ARA&A*, 2, 213. doi:10.1146/annurev.aa.02.090164.001241
- Bouma, L., Hartman, J., Bhatti, W., Winn, J., Bakos, G., 2019, *ApJS*, 245, 13. doi:10.17909/t9-ayd0-k727
- Bowler, B. P., Hinkley, S., Ziegler, C., et al. 2019, *ApJ*, 877, 60. doi:10.3847/1538-4357/ab1018
- Broeg, C., Schmidt, T. O. B., Guenther, E., et al. 2007, *A&A*, 468, 1039. doi:10.1051/0004-6361/20066793
- Burke, C. J., Levine, A., Fausnaugh, M., Vanderspek, R., Barclay, T., Libby-Roberts, J. E., Morris, B., Sipocz, B., Owens, M., Feinstein, A. D., Camacho, J., 2020, 0.4.1, *Astrophysics Source Code Library*, record ascl:2003:001
- Capak, P., 2013, *Spitzer Enhanced Imaging Products (SEIP) Source List*, IRSA, doi:10.26131/IRSA3
- Cardelli, J. A., Clayton, G. C., & Mathis, J. S. 1989, *ApJ*, 345, 245. doi:10.1086/167900
- Carpenter, J. M., Bouwman, J., Mamajek, E. E., et al. 2009, *ApJS*, 181, 197. doi:10.1088/0067-0049/181/1/197
- CatWISE team, 2020, *CatWISE Preliminary Catalog*, IPAC, doi: 10.26131/IRSA126
- Chambers, K., Magnier, E., Metcalf, N., et al., 2016, arXiv:1612.05560
- Chen, C. H., Mittal, T., Kuchner, M., et al. 2014, *ApJS*, 211, 25. doi:10.1088/0067-0049/211/2/25
- Christiansen, J. L., Derekas, A., Kiss, L. L., et al. 2008, *MNRAS*, 385, 1749. doi:10.1111/j.1365-2966.2008.13013.x
- Cody, A. M. & Hillenbrand, L. A. 2018, *AJ*, 156, 71. doi:10.3847/1538-3881/aacead
- Cody, A. M., Stauffer, J., Baglin, A., et al. 2014, *AJ*, 147, 82. doi:10.1088/0004-6256/147/4/82
- Cody, A. M., Hillenbrand, L. A., David, T. J., et al. 2017, *ApJ*, 836, 41. doi:10.3847/1538-4357/836/1/41
- Coker, C. T., Pinsonneault, M., & Terndrup, D. M. 2016, *ApJ*, 833, 122. doi:10.3847/1538-4357/833/1/122
- Comerón, F., Spezzi, L., & López Martí, B. 2009, *A&A*, 500, 1045. doi:10.1051/0004-6361/200911771
- Cotten, T. H. & Song, I. 2016, *ApJS*, 225, 15. doi:10.3847/0067-0049/225/1/15
- Cruzalèbes, P., Petrov, R. G., Robbe-Dubois, S., et al. 2019, *MNRAS*, 490, 3158. doi:10.1093/mnras/stz2803
- Curtis, J. L., Agüeros, M. A., Matt, S. P., et al. 2020, *ApJ*, 904, 140. doi:10.3847/1538-4357/abbf58
- Damiani, F., Prisinzano, L., Pillitteri, I., et al. 2019, *A&A*, 623, A112. doi:10.1051/0004-6361/201833994
- David, T. J., Hillenbrand, L. A., Gillen, E., et al. 2019, *ApJ*, 872, 161. doi:10.3847/1538-4357/aafe09
- de Zeeuw, P. T., Hoogerwerf, R., de Bruijne, J. H. J., et al. 1999, *AJ*, 117, 354. doi:10.1086/300682
- DENIS team, 1999, *DENIS catalog*, IPAC, doi:10.26131/IRSA478
- Desidera, S., Covino, E., Messina, S., et al. 2015, *A&A*, 573, A126. doi:10.1051/0004-6361/201323168
- Distefano, E., Lanzafame, A. C., Lanza, A. F., et al. 2016, *A&A*, 591, A43. doi:10.1051/0004-6361/201527698
- Donati, J.-F., Gregory, S. G., Alencar, S. H. P., et al. 2012, *MNRAS*, 425, 2948. doi:10.1111/j.1365-2966.2012.21482.x
- Drake, A. J., Djorgovski, S. G., Catelan, M., et al. 2017, *MNRAS*, 469, 3688. doi:10.1093/mnras/stx1085
- Eisenhardt, P. R. M., Marocco, F., Fowler, J. W., et al. 2020, *ApJS*, 247, 69. doi:10.3847/1538-4365/ab7f2a
- Epchtein, N., Deul, E., Derriere, S., et al. 1999a, *A&A*, 349, 236
- Faherty, J. K., Bochanski, J. J., Gagné, J., et al. 2018, *ApJ*, 863, 91. doi:10.3847/1538-4357/aac76e
- Feinstein, A. D., Montet, B. T., Foreman-Mackey, D., et al. 2019, *PASP*, 131, 094502. doi:10.1088/1538-3873/ab291c
- Fruth, T., Cabrera, J., Chini, R., et al. 2013, *AJ*, 146, 136. doi:10.1088/0004-6256/146/5/136
- Gaia Collaboration, Brown, A. G. A., Vallenari, A., et al. 2016a, *A&A*, 595, A2. doi:10.1051/0004-6361/201629512
- Gaia Collaboration, Brown, A. G. A., Vallenari, A., et al. 2016b, *Gaia Catalog DR1*, IRSA, doi:10.26131/IRSA16
- Gaia Collaboration, Brown, A. G. A., Vallenari, A., et al. 2018a, *A&A*, 616, A1. doi:10.1051/0004-6361/201833051
- Gaia Collaboration, Brown, A. G. A., Vallenari, A., et al. 2018b, *Gaia Source Catalog DR2*. doi:10.26131/IRSA12
- Gaia Collaboration, Brown, A. G. A., Vallenari, A., et al. 2021, *A&A*, 649, A1. doi:10.1051/0004-6361/202039657
- Galli, P. A. B., Bertout, C., Teixeira, R., et al. 2015, *A&A*, 580, A26. doi:10.1051/0004-6361/201525804
- Galli, P. A. B., Bertout, C., Teixeira, R., et al. 2013, *A&A*, 558, A77. doi:10.1051/0004-6361/201220704
- Ghosh, P., Lamb, F. K., & Pethick, C. J. 1977, *ApJ*, 217, 578. doi:10.1086/155606
- Girard, T. M., van Altena, W. F., Zacharias, N., et al. 2011, *AJ*, 142, 15. doi:10.1088/0004-6256/142/1/15
- Godoy-Rivera, D., Pinsonneault, M. H., & Rebull, L. M. 2021, *ApJS*, 257, 46. doi:10.3847/1538-4365/ac2058
- Goldman, B., Röser, S., Schilbach, E., et al. 2018, *ApJ*, 868, 32. doi:10.3847/1538-4357/aae64c
- Günther, M. N., Berardo, D. A., Ducrot, E., et al. 2022, *AJ*, 163, 144. doi:10.3847/1538-3881/ac503c
- Henden, A. A., Templeton, M., Terrell, D., et al. 2016, *VizieR Online Data Catalog*, II/336
- Howell, S. B., Sobek, C., Haas, M., et al. 2014, *PASP*, 126, 398. doi:10.1086/676406

- Huang, C. X., Vanderburg, A., Pál, A., et al. 2020, *Research Notes of the American Astronomical Society*, 4, 204. doi:10.3847/2515-5172/abca2e
- Huang, C. X., Vanderburg, A., Pál, A., et al. 2020, *Research Notes of the American Astronomical Society*, 4, 206. doi:10.3847/2515-5172/abca2d
- Indebetouw, R., Mathis, J. S., Babler, B. L., et al. 2005, *ApJ*, 619, 931. doi:10.1086/426679
- Jang-Condell, H., Chen, C. H., Mittal, T., et al. 2015, *ApJ*, 808, 167. doi:10.1088/0004-637X/808/2/167
- Jayasinghe, T., Kochanek, C. S., Stanek, K. Z., et al. 2018, *MNRAS*, 477, 3145. doi:10.1093/mnras/sty838
- Joy, A. H. 1945, *ApJ*, 102, 168. doi:10.1086/144749
- Kapteyn, J. C. 1914, *ApJ*, 40, 43. doi:10.1086/142098
- Kerr, R. M. P., Rizzuto, A. C., Kraus, A. L., et al. 2021, *ApJ*, 917, 23. doi:10.3847/1538-4357/ac0251
- Kiraga, M. 2012, *AcA*, 62, 67
- Koenigl, A. 1991, *ApJL*, 370, L39. doi:10.1086/185972
- Kóspál, Á., Mohler-Fischer, M., Sicilia-Aguilar, A., et al. 2014, *A&A*, 561, A61. doi:10.1051/0004-6361/201322428
- Kounkel, M. & Covey, K. 2019, *AJ*, 158, 122. doi:10.3847/1538-3881/ab339a
- Kraus, A. L. & Hillenbrand, L. A. 2009, *ApJ*, 704, 531. doi:10.1088/0004-637X/704/1/531
- Kraus, A. L., Herczeg, G. J., Rizzuto, A. C., et al. 2017, *ApJ*, 838, 150. doi:10.3847/1538-4357/aa62a0
- Lasker, B. M., Lattanzi, M. G., McLean, B. J., et al. 2008, *AJ*, 136, 735. doi:10.1088/0004-6256/136/2/735
- Liu, J., Fang, M., & Liu, C. 2020, *AJ*, 159, 105. doi:10.3847/1538-3881/ab6b22
- Luhman, K. L. 2022, *AJ*, 163, 25. doi:10.3847/1538-3881/ac35e3
- Luhman, K. L. 2022, *AJ*, 163, 24. doi:10.3847/1538-3881/ac35e2
- Luhman, K. L. & Mamajek, E. E. 2012, *ApJ*, 758, 31. doi:10.1088/0004-637X/758/1/31
- Marton, G., Calzoletti, L., Perez Garcia, A. M., et al. 2017, *arXiv:1705.05693*
- Mathis, J. S. 1990, *ARA&A*, 28, 37. doi:10.1146/annurev.aa.28.090190.000345
- Meisner, A. M., Lang, D., Schlafly, E. F., et al. 2019, *PASP*, 131, 124504. doi:10.1088/1538-3873/ab3df4
- Mellon, S. N., Mamajek, E. E., Oberst, T. E., et al. 2017, *ApJ*, 844, 66. doi:10.3847/1538-4357/aa77fb
- Messina, S., Desidera, S., Turatto, M., et al. 2010, *A&A*, 520, A15. doi:10.1051/0004-6361/200913644
- Messina, S., Desidera, S., Lanzafame, A. C., et al. 2011, *A&A*, 532, A10. doi:10.1051/0004-6361/201016116
- Meyer, M. R., Calvet, N., & Hillenbrand, L. A. 1997, *AJ*, 114, 288. doi:10.1086/118474
- Meyer, M. R., Hillenbrand, L. A., Backman, D., et al. 2006, *PASP*, 118, 1690. doi:10.1086/510099
- Mittal, T., Chen, C. H., Jang-Condell, H., et al. 2015, *ApJ*, 798, 87. doi:10.1088/0004-637X/798/2/87
- Moolekamp, F. E., Mamajek, E. E., James, D. J., et al. 2019, *MNRAS*, 484, 5049. doi:10.1093/mnras/stz183
- Murakami, H., Baba, H., Barthel, P., et al. 2007, *PASJ*, 59, S369. doi:10.1093/pasj/59.sp2.S369
- Nicholson, B. A., Hussain, G. A. J., Donati, J.-F., et al. 2018, *MNRAS*, 480, 1754. doi:10.1093/mnras/sty1965
- Oh, S., Price-Whelan, A. M., Brewer, J. M., et al. 2018, *ApJ*, 854, 138. doi:10.3847/1538-4357/aaab4d
- Pecaut, M. J., Mamajek, E. E., & Bubar, E. J. 2012, *ApJ*, 746, 154. doi:10.1088/0004-637X/746/2/154
- Pecaut, M. J. & Mamajek, E. E. 2013, *ApJS*, 208, 9. doi:10.1088/0067-0049/208/1/9
- Pecaut, M. J. & Mamajek, E. E. 2016, *MNRAS*, 461, 794. doi:10.1093/mnras/stw1300
- Pilbratt, G. L., Riedinger, J. R., Passvogel, T., et al. 2010, *A&A*, 518, L1. doi:10.1051/0004-6361/201014759
- Popinchalk, M., Faherty, J. K., Kiman, R., et al. 2021, *ApJ*, 916, 77. doi:10.3847/1538-4357/ac0444
- Preibisch, T. & Smith, M. D. 1997, *A&A*, 322, 825
- Press, W. H., Teukolsky, S. A., Vetterling, W. T., et al. 1992, *Cambridge: University Press*, —c1992, 2nd ed.
- Rampalli, R., Agüeros, M. A., Curtis, J. L., et al. 2021, *ApJ*, 921, 167. doi:10.3847/1538-4357/ac0c1e
- Rebull, L. M. 2001, *AJ*, 121, 1676. doi:10.1086/319393
- Rebull, L. M., Wolff, S. C., & Strom, S. E. 2004, *AJ*, 127, 1029. doi:10.1086/380931
- Rebull, L. M., Stauffer, J. R., Megeath, S. T., et al. 2006, *ApJ*, 646, 297. doi:10.1086/504865
- Rebull, L. M., Stauffer, J. R., Bouvier, J., et al. 2016a, *AJ*, 152, 113. doi:10.3847/0004-6256/152/5/113
- Rebull, L. M., Stauffer, J. R., Bouvier, J., et al. 2016b, *AJ*, 152, 114. doi:10.3847/0004-6256/152/5/114
- Rebull, L. M., Stauffer, J. R., Hillenbrand, L. A., et al. 2017, *ApJ*, 839, 92. doi:10.3847/1538-4357/aa6aa4
- Rebull, L. M., Stauffer, J. R., Cody, A. M., et al. 2018, *AJ*, 155, 196. doi:10.3847/1538-3881/aab605
- Rebull, L. M., Stauffer, J. R., Cody, A. M., et al. 2020, *AJ*, 159, 273. doi:10.3847/1538-3881/ab893c
- Rebull, L. M., Stauffer, J. R., Cody, A. M., et al. 2021, *AJ*, 162, 172. doi:10.3847/1538-3881/ac205f
- Ribas, Á., Merín, B., Bouy, H., et al. 2014, *A&A*, 561, A54. doi:10.1051/0004-6361/201322597
- Ribas, Á., Bouy, H., & Merín, B. 2015, *A&A*, 576, A52. doi:10.1051/0004-6361/201424846

- Ricker, G. R., Winn, J. N., Vanderspek, R., et al. 2015, *Journal of Astronomical Telescopes, Instruments, and Systems*, 1, 014003. doi:10.1117/1.JATIS.1.1.014003
- Ripepi, V., Balona, L., Catanzaro, G., et al. 2015, *MNRAS*, 454, 2606. doi:10.1093/mnras/stv2221
- Ripepi, V., Molinaro, R., Musella, I., et al. 2019, *A&A*, 625, A14. doi:10.1051/0004-6361/201834506
- Samus', N. N., Kazarovets, E. V., Durlevich, O. V., et al. 2017, *Astronomy Reports*, 61, 80. doi:10.1134/S1063772917010085
- Scholz, A., Kostov, V., Jayawardhana, R., et al. 2015, *ApJL*, 809, L29. doi:10.1088/2041-8205/809/2/L29
- Scholz, A., Moore, K., Jayawardhana, R., et al. 2018, *ApJ*, 859, 153. doi:10.3847/1538-4357/aabfbc
- Scargle, J. D. 1982, *ApJ*, 263, 835. doi:10.1086/160554
- Siwak, M., Ogloza, W., Rucinski, S. M., et al. 2016, *MNRAS*, 456, 3972. doi:10.1093/mnras/stv2848
- Skiff, B. A. 2014, *VizieR Online Data Catalog*, B/mk
- Skrutskie, M. F., Cutri, R. M., Stiening, R., et al. 2006, *AJ*, 131, 1163. doi:10.1086/498708
- Skrutskie, M. F., Cutri, R. M., Stiening, R., et al. 2003, *2MASS All-Sky Point Source Catalog*, IPAC, doi:10.26131/IRSA2
- Stauffer, J. R. & Hartmann, L. W. 1987, *ApJ*, 318, 337. doi:10.1086/165371
- Stauffer, J. R., Hartmann, L. W., & Jones, B. F. 1989, *ApJ*, 346, 160. doi:10.1086/167996
- Stauffer, J., Cody, A. M., Baglin, A., et al. 2014, *AJ*, 147, 83. doi:10.1088/0004-6256/147/4/83
- Stauffer, J., Cody, A. M., McGinnis, P., et al. 2015, *AJ*, 149, 130. doi:10.1088/0004-6256/149/4/130
- Stauffer, J., Cody, A. M., Rebull, L., et al. 2016, *AJ*, 151, 60. doi:10.3847/0004-6256/151/3/60
- Stauffer, J., Rebull, L., Bouvier, J., et al. 2016, *AJ*, 152, 115. doi:10.3847/0004-6256/152/5/115
- Stauffer, J., Collier Cameron, A., Jardine, M., et al. 2017, *AJ*, 153, 152. doi:10.3847/1538-3881/aa5eb9
- Stauffer, J., Rebull, L., David, T. J., et al. 2018, *AJ*, 155, 63. doi:10.3847/1538-3881/aaa19d
- Stauffer, J., Rebull, L. M., Cody, A. M., et al. 2018, *AJ*, 156, 275. doi:10.3847/1538-3881/aae9ec
- Stassun, K. G., Oelkers, R. J., Pepper, J., et al. 2018, *AJ*, 156, 102. doi:10.3847/1538-3881/aad050
- Stassun, K. G., Oelkers, R. J., Paegert, M., et al. 2019, *AJ*, 158, 138. doi:10.3847/1538-3881/ab3467
- Strassmeier, K. G., Rice, J. B., Ritter, A., et al. 2005, *A&A*, 440, 1105. doi:10.1051/0004-6361:20052901
- Tajiri, T., Kawahara, H., Aizawa, M., et al. 2020, *ApJS*, 251, 18. doi:10.3847/1538-4365/abbc17
- unWISE team, 2019, unWISE catalog, IRSA, doi:10.26131/IRSA525
- Werner, M. W., Roellig, T. L., Low, F. J., et al. 2004, *ApJS*, 154, 1. doi:10.1086/422992
- Wright, E. L., Eisenhardt, P. R. M., Mainzer, A. K., et al. 2010, *AJ*, 140, 1868. doi:10.1088/0004-6256/140/6/1868
- Wright, E. L., Eisenhardt, P. R. M., Mainzer, A. K., et al. 2010, *AllWISE Source Catalog*, doi:10.26131/IRSA1
- Wright, N. J. & Mamajek, E. E. 2018, *MNRAS*, 476, 381. doi:10.1093/mnras/sty207
- Zacharias, N., Monet, D. G., Levine, S. E., et al. 2004, *AAS Meeting Abstracts*
- Zari, E., Hashemi, H., Brown, A. G. A., et al. 2018, *A&A*, 620, A172. doi:10.1051/0004-6361/201834150
- Zhan, Z., Günther, M. N., Rappaport, S., et al. 2019, *ApJ*, 876, 127. doi:10.3847/1538-4357/ab158c
- Zúñiga-Fernández, S., Bayo, A., Elliott, P., et al. 2021, *A&A*, 645, A30. doi:10.1051/0004-6361/202037830

Table 3. Contents of Table: Periods and Supporting Data for Discarded/Rejected Sources

Number	Label	Contents
1	TIC	Number in the <i>TESS</i> Input Catalog (TIC)
2	coord	Coordinate-based (right ascension and declination, J2000) name for target
3	othername	Alternate name for target
4	gaiaid	Gaia DR2 ID
5	distance	Distance from Bailer-Jones et al. (2018) in parsecs
6	Kmag	K_s magnitude (in Vega mags), if observed
7	vmk-used	$(V - K_s)$ used, in Vega mags (observed or inferred; see text)
8	evmk	$E(V - K_s)$ adopted for this star (in mags; see § 3.3)
9	Kmag0	dereddened $K_{s,0}$ magnitude (in Vega mags), as inferred (see §3.3)
10	vmk0	$(V - K_s)_0$, dereddened $V - K_s$ (in Vega mags), as inferred (see § 3.3; rounded to nearest 0.1 to emphasize the relatively low accuracy)
11	color_uncertcode	two digit uncertainty code denoting origin of $(V - K_s)$ and $(V - K_s)_0$ (see §3.1 and 3.3): First digit (origin of $(V - K_s)$): 1= V measured directly from the literature (including SIMBAD) and K_s from 2MASS; 2= V from the literature (see §3.1) and K_s from 2MASS; 3= $(V - K_s)$ inferred from Gaia DR1 G and K_s from 2MASS (see §3.1); 4= $(V - K_s)$ inferred from Pan-STARRS1 g and K_s from 2MASS (see §3.1); 6= V inferred from well-populated optical SED and K_s from 2MASS (see §3.1); 7= $(V - K_s)$ inferred from Gaia DR2 G and K_s from 2MASS (see §3.1); -9= no measure of $(V - K_s)$. Second digit (origin of $E(V - K_s)$ leading to $(V - K_s)_0$): 1=dereddening from JHK_s diagram (see §3.3); 2=dereddening back to $(V - K_s)_0$ expected for spectral type; 3=dereddening from SED fits; 4=used median $E(V - K_s)=0$ (see §3.3); -9= no measure of $E(V - K_s)$
12	P1	Primary period, in days (taken to be rotation period in cases where there is > 1 period)
13	P2	Secondary period, in days
14	P3	Tertiary period, in days
15	P4	Quaternary period, in days
16	p_uncertcode	uncertainty code for period – is there any reason to worry about this period? Values are ‘n’ (no worry, full confidence; by far the most common value), ‘(n)’ (no period), and then ‘n?’ and ‘y?’ are progressively less confident periods.
17	IRexcess	Whether an IR excess is present or not (see §3.4)
18	IRexcessStart	Minimum wavelength at which the IR excess is detected or the limit of our knowledge of where there is no excess (see §3.4)
19	SEDslope	best-fit slope to all detections between 2 and 25 microns
20	SEDclass	SED class (I, flat, II, or III) based on the SED slope between 2 and 25 microns
21	dipper	LC matches dipper characteristics (see §4.5)
22	burster	LC matches burster characteristics (see §4.5)
23	single/multi-P	single or multi-period star
24	dd	LC and power spectrum matches double-dip characteristics (see §4.5)
25	ddmoving	LC and power spectrum matches moving double-dip characteristics (see §4.5)
26	shapechanger	LC matches shape changer characteristics (see §4.5)
27	beater	LC has beating visible (see §4.5)
28	complexpeak	power spectrum has a complex, structured peak and/or has a wide peak (see §4.5)
29	resolvedclose	power spectrum has resolved close peaks (see §4.5)
30	resolveddist	power spectrum has resolved distant peaks (see §4.5)
31	pulsator	power spectrum and LC match pulsator characteristics (see §4.5)
32	scallop	LC matches scallop or flux dip characteristics (see §4.5 and App. C)
33	EB	LC has characteristics of eclipsing binary (see §4.5 and App. C)

APPENDIX

A. REJECTED/DISCARDED SOURCES

As mentioned in detail in the main body of the paper, there are sources that we have discarded from the analysis above for any of a number of reasons, ranging from not having a *TESS* LC at all or not having a *TESS* LC that was uncontaminated, to not having a V or a K_s , or other reasons. This appendix largely consists of the table of values for these discarded sources, should later investigators wish to use any of this information. Note that the periods are right for the LCs that we have, but the LCs **often do not correspond to the stars listed here**; the most common reason we have for rejecting a source is that there is obvious source confusion in the *TESS* LCs.

Table 4. Contents of Table: Comparison to Literature Periods

Number	Label	Contents
1	tic	TIC number
2	catnum	Position-based catalog number
3	pkiraga	P in days from Kiraga (2012)
4	pmellon	P in days from Mellon et al. (2017)
5	pgdr2	P in days from Gaia DR2
6	pasasn	P in days from ASAS-SN
7	plit	P in days from elsewhere in the literature
8	pcite	citation for literature source of P in col 7
9	p1	first period reported here
10	p2	second period reported here
11	p3	third period reported here
12	p4	fourth period reported here
13	match?	is this a match?
14	notes	notes

B. COMPARISON TO LITERATURE PERIODS

Section 4.4 discussed in broad terms the comparison of our period finding to that from the literature. In this appendix, we list periods for ~ 600 specific stars in common between our study and several literature studies, regardless of whether or not the stars are currently thought to be UCL/LCC members or not. The stars are listed in Table 4. If the *TESS* period matches the literature period within 15%, we take it as a match. If the *TESS* period is a match between 15 and 20%, we take it as close but not quite a match. Several periods are too long for *TESS* to have recovered. In a few cases, the literature period matches a provisional period identified in *TESS* or in the literature; in some additional cases, there is a peak in *TESS* at or near the literature P , but we had discarded the *TESS* P as unlikely to be astrophysical and/or more likely to be a timescale than a rotation period. See the notes in the table.

C. UNUSUAL LCS

As discussed in Sec. 4.5, most of the LCs considered here are well-behaved, e.g., sinusoidal and clearly periodic (or clearly not), and the periodic signal is easily interpreted as the rotation of the star. However, there are ~ 150 stars ($< 4\%$ of the entire sample) that we wanted to call out here because they are unusual in some way. They are all listed in Table 5 with notes as to why they merited listing here. Parameters for all of them (including periods) are listed in the big data tables above; this table here is largely notes on these stars. The table includes TIC number, coordinate-based name, what member sample they are in (gold, silver, bronze, or reject), how confident we are that they should be in the category we have placed them (e.g., scallop or EB, etc.) and whether or not the detected period is due to rotation, and any additional notes about them. In the context of the entire sample (or the entire member sample), there are very few for which we are not confident about the bin in which we have placed them, and errors in their categorization doesn't affect any of our conclusions. More detailed, statistical characterization of any of these stars or categories is beyond the scope of the present paper, so they are simply listed here.

This list includes scallops and flux dips published in Stauffer et al. (2021), two of which have had to be rejected here due to source confusion; it also includes new scallops and flux dips identified here, as well as stars that may be scallops or flux dips but that are lower signal-to-noise.

Also in the table are candidate pulsators, including some that have phased waveforms that resemble a 'ski jump' – e.g., they look like those of RR Lyr, but these are, in general, very fast (hours). For the pulsators, note that their periods appear in the tables above, but they are omitted from the plots involving P_{rot} , since they are not rotation.

Many obvious eclipsing binaries (EBs) appear in the LCs; some phased LCs could be EBs or could be flux dips, and it's very hard to determine from the available (often low signal-to-noise) LC which one it is. In cases of obvious EBs, we have omitted P_{EB} from plots, but have retained P_{rot} where it was possible to derive a plausible rotation period

estimate from the LC. Of the EBs, about half of them appear above the MS, e.g., consistent with being a binary, in Fig. 9.

Table 5. List of Unusual Objects

TIC	Name	Member bin	sample confidence ^a	notes
405235910	102115.42-622604.3	gold	high but not rotation	pulsator
93952051	102646.51-595526.8	silver	low but not rotation	pulsator?
273703001	103137.10-690158.7	bronze	high but not rotation	pulsator
412006082	103341.80-641345.7	gold	high but not rotation	pulsator
242558208	103422.70-641809.3	silver	high but not rotation	pulsator
351521478	103819.04-612100.7	silver	high but not rotation	pulsator
390470134	103844.36-595443.7	silver	high but not rotation	pulsator
419686932	104122.99-694043.1	silver	high but not rotation	pulsator
92574021	113249.19-494907.8	gold	low	scallop?
451984338	113319.04-594822.0	gold	high but not rotation	EB, only P is that of binary ; $P_{EB}=1.132$
290889135	113556.21-653012.1	gold	high	scallop in p2
280945693	113616.71-692751.8	gold	high	Published as flux dip in Stauffer+21
452345586	113658.55-582237.5	gold	high	flux dip
93763678	114322.41-532711.4	gold	high	flux dip
323478101	114557.95-635246.3	gold	high but not rotation	EB, only P is that of binary ; $P_{EB}=0.477$
296790810	114625.66-664135.6	gold	high	Published as flux dip in Stauffer+21; possible small IR excess
268665785	114902.67-570014.1	gold	low	possible EB; extracted P_{rot}
301432612	115404.70-580241.3	gold	high	Published as scallop in Stauffer+21
307686978	120017.79-635549.0	bronze	high	EB, but can pull out P_{rot} ; $P_{EB}=2.778$
398768350	120119.80-564902.7	gold	high	Published as scallop in Stauffer+21
379774242	120504.18-644721.6	gold	low	scallop?
994964114	120858.09-513019.6	reject	(reject)	source confusion so rejected, but p1 could be a flux dip
994964138	120858.19-513017.2	reject	(reject)	source confusion so rejected, but p1 could be a flux dip
334409011	121318.43-515641.6	gold	high	EB, but can pull out P_{rot} ; $P_{EB}=3.361$
288093002	122028.00-543537.6	gold	high	Published as flux dip in Stauffer+21
310412874	122048.65-640904.1	silver	low	flux dip? Small IR excess
448002486	122138.04-690838.4	gold	high	Published as flux dip in Stauffer+21
310720311	122153.09-634733.9	gold	high	Published as scallop in Stauffer+21
411614400	122201.40-573757.1	gold	high but not rotation	EB, only P is that of binary ; $P_{EB}=1.535$
135162879	122213.16-414802.7	gold	high	Published as scallop in Stauffer+21
311447879	122220.20-650950.6	bronze	low	flux dip?
311333943	122247.22-633757.6	silver	low	flux dip, possible IR excess, possible icicles?
261573174	122303.08-542526.9	silver	low	possible EB; extracted P_{rot} ; $P_{EB}=1.084$
311592558	122348.30-633248.7	silver	low	possible EB; extracted P_{rot}
311585720	122354.75-641730.0	silver	high but not rotation	EB, only P is that of binary ; $P_{EB}=0.612$
450386147	122424.02-645344.0	gold	low	flux dip?
273460357	122500.61-521627.1	reject	(reject)	source confusion so rejected, but an interesting LC shape.
273460338	122501.42-521614.6	reject	(reject)	source confusion so rejected, but an interesting LC shape.
281742840	122504.80-655942.1	bronze	high but not rotation	EB, only P is that of binary ; $P_{EB}=4.760$
271221172	122657.75-554620.0	gold	high but not rotation	EB, only P is that of binary ; $P_{EB}=0.266$
450957950	122902.23-645500.6	gold	high but not rotation	EB, only P is that of binary ; $P_{EB}=2.360$
272407484	123108.44-545644.5	gold	low	flux dip in p2; clear IR excess.
179968331	123410.56-635241.6	gold	high but not rotation	EB, only P is that of binary ; $P_{EB}=2.825$
273821594	123624.97-550710.6	gold	high	scallop and flux dip?
411681763	123742.99-554851.2	gold	high but not rotation	EB, only P is that of binary ; $P_{EB}=1.415$
73183013	123941.30-464444.6	gold	high	three dips per cycle, still sinusoidal

Table 5 continued on next page

Table 5 (continued)

TIC	Name	Member bin	sample confidence ^a	notes
161734785	124147.22-511006.7	gold	high	Published as scallop in Stauffer+21
412182239	124231.62-590512.6	silver	low	Two very clear v-shaped dips per cycle, not evenly spaced. Substantial IR excess & long P (1.3 d), both of which are inconsistent with scallop category. Counted as scallop but..?
328468855	124301.62-675620.8	gold	high	flux dip
419502814	124434.42-551246.5	gold	high	EB, but can pull out P_{rot} ; $P_{\text{EB}}=1.059$
419779703	124631.20-540431.4	gold	high	scallop
405695928	124826.12-553816.1	silver	high	flux dip
405754448	124831.44-594449.8	gold	low	scallop shape but at $(V - K_s)_0 \sim 3$, this is too blue for a scallop, and at $P \sim 0.5$, it is much faster than other stars of its color. Source confusion?
165904363	124942.09-495316.3	gold	high	flux dip
165912675	125033.96-482656.5	gold	low	flux dip?
405970436	125058.63-593400.6	gold	high	scallop
405910532	125100.26-564313.1	reject	(reject)	source confusion so rejected, but could be EB
405910546	125100.61-564321.0	reject	(reject)	source confusion so rejected, but could be EB
412376751	125129.47-592421.7	gold	low	flux dip?
412376096	125137.68-592945.0	bronze	high	flux dip
435899024	125222.75-641839.4	gold	high	Published as scallop in Stauffer+21; possible IR excess
406040223	125521.95-584641.8	gold	high	Published as flux dip in Stauffer+21
248145126	125545.32-445151.7	gold	high	Published as scallop in Stauffer+21; possible IR excess
335598085	125935.63-680801.6	gold	high	Published as scallop in Stauffer+21
253239639	130159.57-592023.8	gold	high but not rotation	'ski jump'; shaped like RR Lyr but very fast
404335106	130317.73-515013.0	gold	low	flux dip, though at ~ 3 days, the period is very long compared to other flux dips.
404387832	130354.33-501502.3	gold	high	scallop
439883940	130416.15-640557.0	silver	high	EB, but can pull out P_{rot} ; $P_{\text{EB}}=6.176$
258583707	130730.60-454919.7	gold	low	flux dip? EB? Counted as flux dip
441263248	130927.70-653325.5	gold	high	EB, but can pull out P_{rot} ; $P_{\text{EB}}=6.877$
245002119	130949.27-513546.3	gold	high but not rotation	EB, only P is that of binary ; $P_{\text{EB}}=0.581$
363656704	131920.44-450800.7	gold	high	EB, but can pull out P_{rot}
973449111	131935.91-623436.9	gold	high	Published as flux dip in Stauffer+21
438709950	132424.75-475730.1	gold	low	flux dip?
243192504	133157.69-470614.9	gold	high	EB, but can pull out P_{rot}
261272259	133521.22-493921.0	bronze	high	EB? Dominant P is P_{rot} , with eclipses
241375625	133852.06-510507.0	gold	high	flux dip in p2
243381460	134001.65-434857.3	gold	high	Published as scallop in Stauffer+21
243449997	134233.80-460826.4	gold	high	flux dip
243499565	134435.82-470613.8	gold	high	Published as flux dip in Stauffer+21
166302995	134518.06-410202.2	gold	low	possible EB; extracted P_{rot} ; $P_{\text{EB}}=2.881$
207621404	134732.79-553301.9	gold	high	Published as scallop in Stauffer+21
243611773	134816.29-440238.8	gold	high	Published as flux dip in Stauffer+21; flux dip in p2
208351772	135345.11-554420.0	silver	high	EB, but can pull out P_{rot} ; $P_{\text{EB}}=5.003$
448165364	135407.42-673344.9	gold	high	three dips per cycle, still sinusoidal
312410638	140146.25-501537.3	gold	high	flux dip
328906141	140554.60-522600.5	gold	high	Published as scallop in Stauffer+21
179368022	140729.83-385427.0	gold	high	scallop in p2
179367270	140731.25-393216.8	gold	high	flux dip, though at ~ 3 days, the period is very long compared to other flux dips.

Table 5 continued on next page

Table 5 (continued)

TIC	Name	Member bin	sample confidence ^a	notes
329694185	140953.34-521717.7	silver	high	scallop
330560000	141424.51-510319.3	gold	high	Published as flux dip in Stauffer+21
242407571	141424.86-455643.6	gold	high	Published as scallop in Stauffer+21; noted has having second period that manifests as "icicles"
330791148	141529.27-495747.5	gold	high	EB? Can pull out P_{rot} ; $P_{\text{EB}}=3.430$
448852739	141605.67-691735.8	gold	high	EB, but can pull out P_{rot}
167448346	142229.54-385517.1	gold	high but not rotation	EB, only P is that of binary ; $P_{\text{EB}}=0.548$
242594123	142347.41-432457.3	gold	high but not rotation	EB, only P is that of binary ; $P_{\text{EB}}=2.548$
241841997	142758.40-392328.7	gold	low	scallop in p3, or possible EB. P3 is <0.5 days, so counted as scallop.
127309526	142759.62-432629.2	gold	high	Published as flux dip in Stauffer+21; flux dip in p2
211513644	142809.56-491545.9	gold	high	Published as flux dip in Stauffer+21
127246012	142829.78-455715.4	gold	high	scallop
241884143	143112.81-410358.6	gold	low	Could be flux dip in p2, could be EB. High enough in CMD to be photometric binary. Counted as flux dip.
127866051	143333.84-474354.5	silver	high	scallop
159427926	143958.40-402809.3	reject	(reject)	source confusion so rejected, but p1 is a flux dip
159427927	143958.71-402809.4	reject	(reject)	source confusion so rejected, but p1 is a flux dip
129116176	144134.97-470029.3	gold	high but not rotation	EB, only P is that of binary ; $P_{\text{EB}}=2.023$
129116164	144139.29-470015.1	silver	high but not rotation	EB, only P is that of binary ; $P_{\text{EB}}=2.019$
129309458	144343.05-433756.0	gold	high	flux dip
309321971	145537.81-493427.7	gold	high	scallop
461643692	145823.13-334415.4	gold	high	Published as flux dip in Stauffer+21
334325329	150031.41-462131.4	gold	high	flux dip
75489110	150033.42-342954.6	gold	high but not rotation	'ski jump' in P2; shaped like RR Lyr but very fast
334838280	150234.31-441933.2	gold	low	flux dip?
121727134	150455.33-375746.9	gold	high but not rotation	EB, contact binary, only P is that of binary ; $P_{\text{EB}}=0.374$
121840452	150516.87-381412.4	gold	high	Published as scallop in Stauffer+21
366178112	150638.97-435728.9	gold	low	possible 'ski jump'? Or flux dip? Unclear.
160539036	150757.83-440458.7	gold	low	flux dip in p2
76048114	150804.78-314231.8	reject	(reject)	source confusion so rejected, but p2 is a scallop
76048113	150805.11-314231.4	reject	(reject)	source confusion so rejected, but p2 is a scallop
140765939	151339.89-434020.8	gold	high	flux dip
276502773	151433.88-405419.8	silver	high	scallop
76698847	151616.51-322309.6	gold	high	flux dip
148218929	151858.60-374518.5	gold	high but not rotation	EB, only P is that of binary ; $P_{\text{EB}}=1.768$
272398365	151903.08-321453.9	gold	high	flux dip
89026133	152234.45-350414.6	reject	(reject)	Published as flux dip in Stauffer+21; possible IR excess; now have to reject for source confusion
89026136	152235.51-350357.7	reject	(reject)	Published as flux dip in Stauffer+21; possible IR excess; now have to reject for source confusion
147828926	152257.19-455619.2	gold	high	scallop
173267960	153758.40-403805.3	gold	high	flux dip in p3
176205621	154212.72-410955.5	gold	high	flux dip
177906792	154426.96-362543.2	gold	low	scallop in p2
254612758	154508.33-442607.9	gold	high	Published as flux dip in Stauffer+21
99207324	154606.01-352510.7	gold	high	Published as flux dip in Stauffer+21

Table 5 continued on next page

Table 5 (*continued*)

TIC	Name	Member bin	sample confidence ^a	notes
179357494	154713.17-411451.1	gold	low	flux dip?
442575691	154802.96-305431.8	gold	low	scallop?
364291454	155607.07-400036.2	gold	low	p1 is ‘ski jump’ (shaped like RR Lyr but very fast); p2 is flux dip.
1172201258	155709.59-320434.2	reject	(reject)	source confusion so rejected, but p1 is a flux dip
1172201260	155709.76-320434.3	reject	(reject)	source confusion so rejected, but p1 is a flux dip
58753591	155758.97-415846.6	gold	high but not rotation	‘ski jump’; shaped like RR Lyr but very fast
279691401	155915.83-365712.3	gold	high but not rotation	‘ski jump’; shaped like RR Lyr but very fast
69874547	160556.03-373748.2	silver	high but not rotation	EB, only P is that of binary ; $P_{EB}=0.795$
4231194	162231.10-410527.8	gold	low	Possible EB ; $P_{EB}= 0.284$
223461868	162508.50-415446.5	silver	high	EB, but can pull out P_{rot} ; $P_{EB}=1.325$
84187344	163854.75-405519.8	silver	low	flux dip? ‘icicle’? $\sim 4d$ period too long for flux dip but does not look like EB.
84756561	163952.56-394431.1	gold	high but not rotation	EB, contact binary, only P is that of binary ; $P_{EB}=0.449$
85125492	164033.61-390722.1	gold	low	flux dip? Blue $((V - K_s)_0 \sim 4)$ for a flux dip, and has a significant IR excess.
85356121	164116.54-382322.8	gold	low	flux dip?
77919426	164400.33-395943.8	gold	high but not rotation	EB, only P is that of binary ; $P_{EB}=1.333$
96140771	164455.86-341043.3	gold	high	EB, but can pull out P_{rot} ; $P_{EB}=1.290$
97239026	164717.49-324535.8	gold	low	scallop?
337253450	165043.59-371212.9	gold	high	EB, but can pull out P_{rot} ; $P_{EB}=1.927$
337243787	165050.98-381226.5	gold	low	flux dip
191694822	165108.97-330059.4	gold	high	EB? Can pull out P_{rot}

^a “Sample confidence” means how confident we are in both the placement in the category (e.g., ‘scallop’ or ‘EB’) and in the measured period being rotation.

D. TIMESCALES

Some LCs have some repeated patterns that we cannot identify with certainty as a rotation period. Table 6 summarizes these timescales for the stars out of the entire ensemble. Note the frequent appearance of 6-8 d timescales (or multiples thereof) – this may be a timescale introduced by *TESS* or the data reduction (see Sec. 4.3).

Table 6. List of Objects with Timescales

TIC	Name	Timescale (d) and/or Notes
0311456083	122327.67-653614.1	2.4? 6.5?
0425319705	124406.63-555418.2	7.5?
0253309679	130350.87-582054.7	15?
0253451463	130713.28-542732.7	6?
0253455154	130807.49-543230.9	8?
0406246159	131022.15-591740.0	5?
0253957851	131600.11-570415.6	6?
0245266758	131723.19-512217.4	2? 5? 14? has IR excess
1048575980	132507.42-430409.8	4? 8? very close to NGC 5128 (Cen A)
0243222122	133408.54-472700.9	15?
0243249579	133419.83-433250.1	4?
0413084801	133908.59-585128.6	7?
1052983805	134132.37-443044.0	20?

Table 6 *continued on next page*

Table 6 (continued)

TIC	Name	Timescale (d) and/or Notes
0275884492	135209.38-433223.6	4?
0241684780	135230.72-515337.2	5? 6?
0208317834	135324.21-574630.0	5? done on portion of LC
0242153310	140108.61-443029.4	8?
0329007676	140639.03-502509.3	5?
0179410344	140809.36-391251.5	6?
0242548815	142119.68-474532.7	7?
0180028859	142123.18-390714.4	7?
0392752922	143120.10-350835.6	4?
0289425666	143749.01-492827.4	7.2?
0159656935	144223.07-404149.7	2? 12?
0159711236	144346.08-371908.9	3? 0.4? done on portion of LC
0159751326	144426.97-415323.0	2? 4? has IR excess
0451276379	144431.39-485707.1	451276379 & 451276381 are confused; 4?
0451276381	144431.74-485710.3	451276379 & 451276381 are confused; 4?
0460218478	144911.31-500114.0	6?
0335145136	150425.51-453050.5	7? 11?
0121932858	150618.61-412016.9	1.3?
0160476756	150708.81-445555.0	6.4?
0160818175	150947.71-461948.4	4?
0185053184	152803.22-260003.4	7?
0054516263	152812.46-343606.0	5?
0153781950	153141.33-472926.2	9? 5?
0171609844	153538.29-410709.2	8?
0172608416	153650.92-384138.6	5?
0290559990	153745.91-423656.8	5? 15?
0254394156	154034.80-445322.3	15?
0178767016	154659.81-395344.3	7? 12?
0179347980	154711.40-392414.4	8?
0179058102	154723.35-364411.6	6? 5?
0442586515	154854.12-351319.2	7?
0442623945	154912.10-353905.5	10? disk LC, and has IR excess
0058245194	155302.65-363305.7	7?
0058170116	155307.05-385500.4	7?
0255260454	155721.11-433342.9	5?
0279883855	155916.48-415710.7	7? disk LC, and has IR excess; burster
0059016771	155958.21-360255.6	12? matches literature!
0059501088	160233.48-362923.4	59501088 & 59501092 are confused; 5?
0059501092	160233.48-362928.3	59501088 & 59501092 are confused; 5?
0257368371	160317.74-421502.5	5? has IR excess
0256901758	160319.73-442214.2	4?
0069514999	160445.05-380512.0	3.5? 7?
0457995946	160854.69-393743.6	disky, 2.4? has IR excess
0382700580	160928.01-384854.2	7?
0382714814	160942.04-405225.4	7?
0164027526	161152.32-420436.2	2?
0004231380	162250.15-410301.2	6?
0225431084	162828.83-444903.2	2? short-P thing seen by eye, cannot recover
0029459205	163121.55-394350.8	7?
0291256981	163308.67-382215.2	8?
0083468373	163741.14-370654.4	8?
0458060193	164156.02-395300.7	6?
0458203191	164212.49-392611.5	7?
0077918101	164426.14-400803.6	7?

Table 6 continued on next page

Table 6 (*continued*)

TIC	Name	Timescale (d) and/or Notes
0078874478	164619.08-392723.8	8?
0337243291	165046.65-381526.2	2?